이학박사 학위논문

Motor control mechanism of brain and brain-machine interface using feedback signals

뇌의 운동제어기전 및 피드백신호를 이용한 뇌-기계 인터페이스에 관한 연구

2017년 2월

서울대학교 대학원
협동과정 뇌과학 전공
염 홍 기

Motor control mechanism of brain and brain-machine interface using feedback signals

지도교수 정 천 기

이 논문을 이학박사 학위논문으로 제출함.
2016년 11월

서울대학교 대학원
협동과정 뇌과학 전공
염 홍 기

염홍기의 이학박사 학위논문을 인준함.
2016년 12월

위 원 장 권 준 수 (인)

부위원장 정 천 기 (인)

위 원 방 문 석 (인)

위 원 김 상 정 (인)

위 원 김 성 필 (인)

ABSTRACT

Motor control mechanism of brain and brain-machine interface using feedback signals

Hong Gi Yeom

Interdisciplinary Program in Neuroscience

The Graduate School

Seoul National University

Introduction: The brain–machine interface (BMI) is a very useful technology that will help disabled people to communicate with others and to control electrical devices. Recent invasive BMI studies showed good results that people with tetraplegia controlled robotic arm to reach and grasp an object using their brain signals. It is very meaningful because lots of thing will be possible if disabled people can control robotic arm like their one. However, invasive method can cause damage to the brain tissue and the method is unstable for long-term recording. Therefore, non-invasive or less-invasive BMI studies to predict movement intentions with high accuracy are

required. Moreover, to use a BMI system in real life, users should be able to change the mode of the system according to their needs.

Method: First, I developed a signal processing algorithm to predict 3-dimensional arm movements from non-invasive MEG signals. MEG signals were acquired during center-out goal-directed reaching movements from nine healthy subjects. Movement-related features were extracted from MEG signals based on several analyses. Multiple linear regression (MLR) was used to estimate movement velocities. Second, I developed an algorithm to compensate the prediction using feedback signals to increase the BMI performance accuracy. The algorithm predicts the target among objects based on the predicted direction and modifies the predicted movement trajectories toward the target to easily reach the target. Third, I investigated the transition of brain connectivity during reaching that can be used to detect brain state to change the BMI mode. Mutual information (MI) was calculated as a functional connectivity according to the time flow. Finally, I proposed the direction of future BMI system based on the study results.

Results: Movement velocities could be estimated from the low-frequency MEG signals (0.5–8 Hz) with significant and considerably high accuracy ($p < 0.001$, mean $r > 0.7$). The accuracy of the movement prediction was significantly improved for all subjects ($p < 0.001$) and 32.1% of the mean error was reduced using feedback signals. Brain connectivity changed according to the brain state. Moreover, centralities on most of motor related areas increased before the movement onset, whereas centralities

only on cerebellum and basal ganglia increased during the movement.

Conclusion: Movement trajectories can be predicted from non-invasive MEG signals. Moreover, BMI performance can be highly increased using feedback information. Because the brain connectivities were significantly different during resting, motor planning and execution, the BMI mode will be adjustable using connectivity. Therefore, combining brain states and feedback information may make practical BMI possible.

Key words: Brain-machine interface (BMI), movement trajectory prediction, compensation using feedback, motor control mechanism, functional connectivity.

Student Number: 2011-30131

CONTENTS

LIST OF TABLES

Chapter 1: Introduction

LIST OF FIGURES

Chapter 1: Introduction

Chapter 2: Movement Trajectory Prediction

Chapter 3: Prediction Compensation

Chapter 4: Transition of Brain Connectivity

Chapter 5: Conclusion

LIST OF ABBREVIATIONS

ACC, anterior cingulate cortex

BCI, brain-computer interface

BG, basal ganglia

BMI, brain–machine interface

CAR, common average reference

CB, cerebellum

CNS, central nervous system

CWT, continuous wavelet transform

ECoG, electrocorticography

EEG, electroencephalography

ERD, desynchronization

ERS, event-related synchronization

FPA, feedback-prediction algorithm

ICA, independent component analysis

LFP, local field potential

M1, primary motor cortex

ME, movement error

MEG, magnetoencephalography

MI, mutual information

MLE, maximum likelihood estimation

MLR, multiple linear regression

MRP, movement-related potential

MV, movement variability

OFC, optimal feedback control

PAL, pallidum

PDF, probabilistic density function

PF, prefrontal area

PM, premotor

PMd, dorsal premotor

PNS, peripheral nervous system

PPC, posterior parietal cortex

PUT, putamen

ROI, region of interest

S1, primary somatosensory cortex

SEM, standard error of the mean

SMA, supplementary motor area

SMR, sensorimotor rhythms

SNR, signal-to-noise ratio

SSVEP, steady state visually evoked potential

STG, superior temporal gyrus

SVD, singular value decomposition

THA, thalamus

tSSS, spatiotemporal signal space separation

V1, primary visual cortex

Chapter 1: Introduction

To develop brain–machine interface (BMI) or brain-computer interface (BCI) technology, broad background knowledge is required such as neuroscience, machine learning, signal processing and programing. In this chapter, I will briefly introduce the basic concepts related to the BMIs.

1.1. Basic of Neuroscience

1.1.1. Organization of Human Nerve System

Human nerve system is conventionally divided into two systems that are **central nervous system (CNS)** and **peripheral nervous system (PNS)** (Table 1-1) (Purves, 2008). CNS is classified again into **brain** and **spinal cord**. PNS comprises the **sensory components** and **motor components**. Internal and external stimuli are conveyed to the CNS through the sensory components of the PNS and the CNS sends motor commands to the motor components of the PNS (Fig. 1-1). The process makes us feel sensation and react to the environments. The brain contains **cerebrum**, **cerebellum** and **brain stem**. The cerebrum includes **frontal lobe**, **parietal lobe**, **occipital lobe** and **temporal lobe**. These lobes are also segregated anatomically or functionally. Each part of the cerebral cortex has its function. For example, Broca's area in the

frontal lobe is related to function of speech production (Kennison). Whereas Wernicke's area in the posterior section of the superior temporal gyrus (STG) is involved in the understanding of language. Moreover, primary motor cortex (M1) is related to the motor function and primary sensory cortex (S1) is involved in sensation. Different parts of M1 or S1 are responsible for movement or sensation of different body, respectively (Fig. 1-2). Different parts of the brain are interacted each other through lots of fibers such as projection fibers linking top and down, association fibers linking forward and backward and commissural fibers linking left and right hemispheres.

Table 1. Organization of Human Nerve System

<table>
<tr><td rowspan="9">Nerve system</td><td rowspan="7">CNS</td><td rowspan="6">Brain</td><td rowspan="4">Cerebrum</td><td>Frontal lobe</td></tr>
<tr><td>Parietal lobe</td></tr>
<tr><td>Occipital lobe</td></tr>
<tr><td>Temporal lobe</td></tr>
<tr><td colspan="2">Cerebellum</td></tr>
<tr><td colspan="2">Brain stem</td></tr>
<tr><td colspan="3">Spinal cord</td></tr>
<tr><td rowspan="2">PNS</td><td colspan="3">Sensory components</td></tr>
<tr><td colspan="3">Motor components</td></tr>
</table>

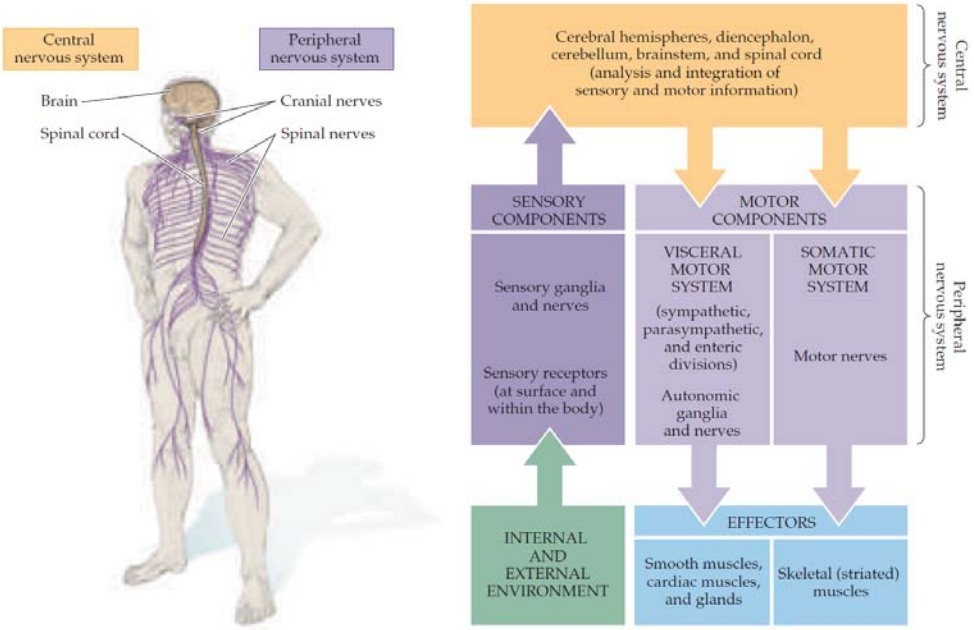

Figure 1-1. Nerve system and functional relationships. Internal and external stimuli are conveyed to the CNS through the sensory components of the PNS and the CNS sends motor commands to the motor components of the PNS. The process makes us feel sensation and react to the environments (Purves, 2008).

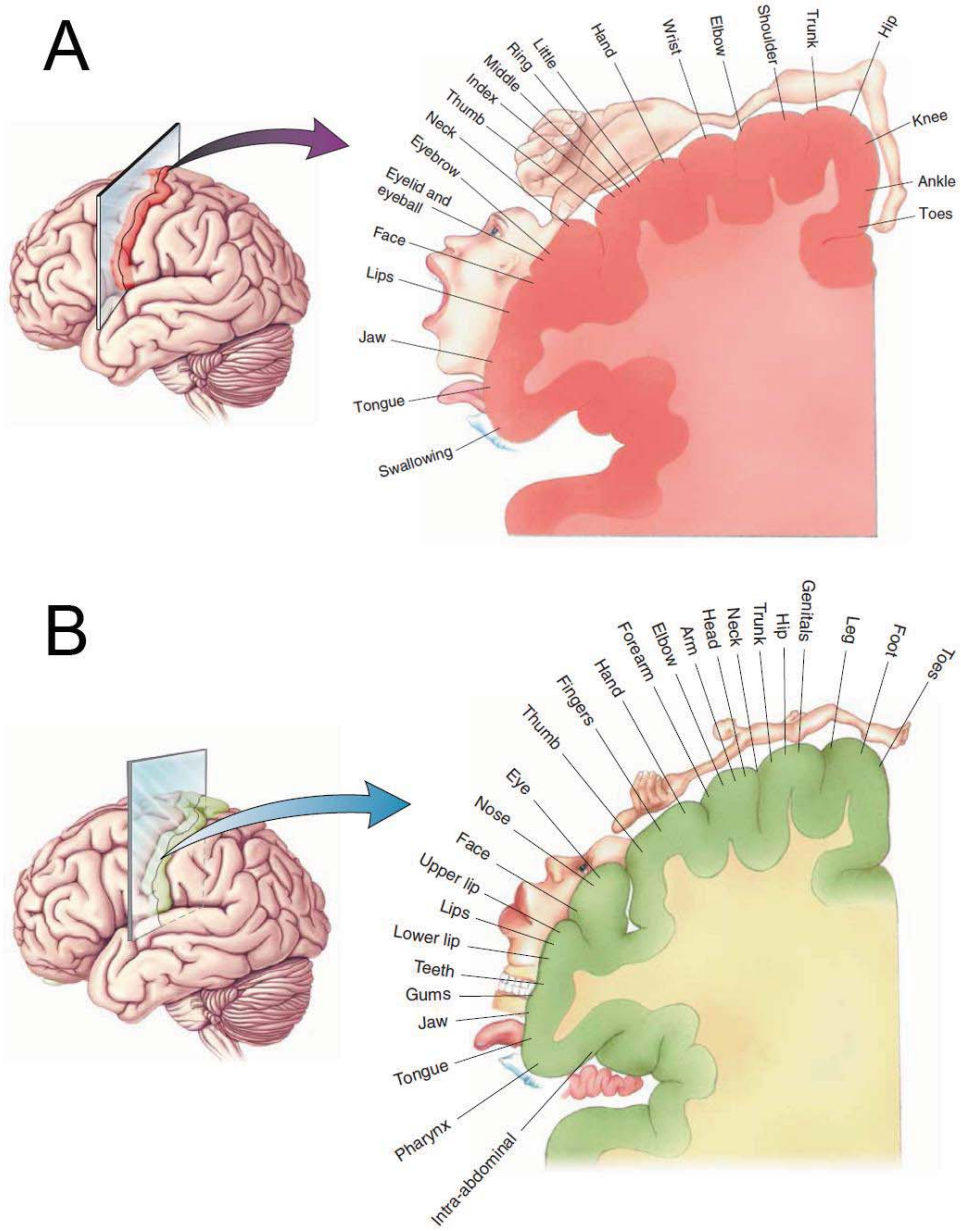

Figure 1-2. Somatotopic map which is also known as homunculus. (A) A somatotopic map of the primary motor cortex (M1). (B) A somatotopic map of the primary somatosensory cortex (S1).

The brain consists of two main classes of cells: **neurons (nerve cells)** and **glia (glial cells)** (Kandel et al., 2013). Neurons are involved in signal processing and transmission, whereas glia support neurons. The human brain contains approximately 100 billion neurons. Neurons typically have four parts: **cell body**, **dendrites**, **axon** and **presynaptic terminals** (Fig. 1-3) (Kandel et al., 2013). Neurons receive signals from other neurons by dendrites. Cell body computes whether the sum of delivered signals is greater than threshold. If the summation is bigger than threshold, action potentials are generated and transmitted to other neurons through axon and presynaptic terminals. Neurons generally have connections with others more than 1,000. The number of action potentials per one second is called firing rate. The neurons generate action potentials with different firing rates according to the different input. Therefore, the firing rate is an important value to understand the neuronal function.

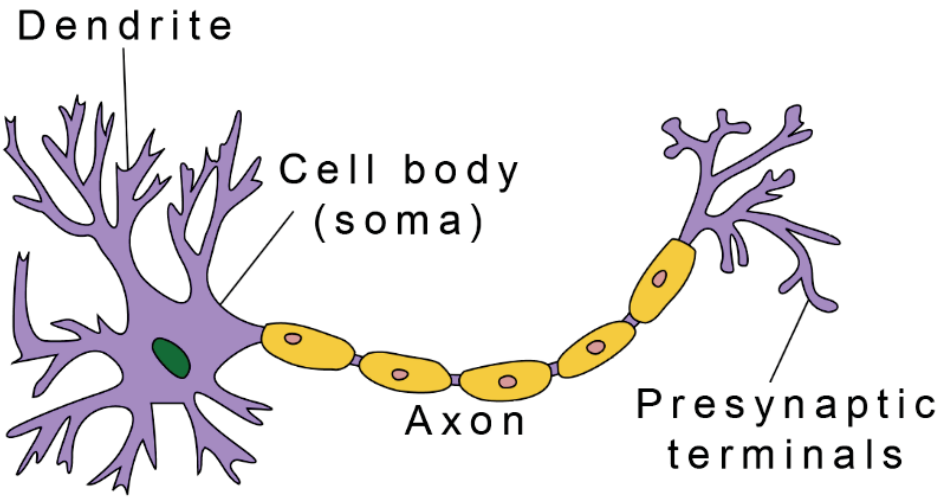

Figure 1-3. Organization of a neuron. Neurons typically have four parts: cell body, dendrites, axon and presynaptic terminals. Neurons receive signals from other neurons by dendrites. Cell body computes whether the sum of delivered signals is greater than threshold. If the summation is bigger than threshold, action potentials are generated and transmitted to other neurons through axon and presynaptic terminals.

1.1.2. Motor Control of Brain

Movements can be categorized as reflexes, rhythmic movements and voluntary movements (Kandel et al., 2013). **Reflexes** are responses to stimuli that cannot be controlled voluntarily. Reflexes are generated by spinal cord or brain stem. **Rhythmic movements** such as locomotion are repetitive and stereotyped movement. Although the rhythmic movements can be controlled voluntarily, the movements are usually controlled autonomously by spinal cord or brain stem. Whereas **voluntary movements** are under conscious control by the brain.

Motor systems under conscious control have a functional hierarchy (Kandel et al., 2013). The high level of the hierarchy deals with the purpose of a movement. Prefrontal cortex is related to the level. The middle level determines a motor planning. Posterior parietal cortex, supplementary motor area (SMA) and premotor (PM) areas are involved in the level. The lowest level defines movement details such as muscle contractions and movement velocity. This level is controlled by M1, brain stem, and spinal cord.

To achieve goal-directed movements, visual information is delivered through primary visual cortex (V1) and posterior parietal cortex (PPC) (Fig. 1-4). Sensory feedback is also transmitted by S1. PM and SMA plan movements and M1 executes the movements. Basal ganglia (BG) and cerebellum (CB) are also involved in motor control through interaction with other motor related area.

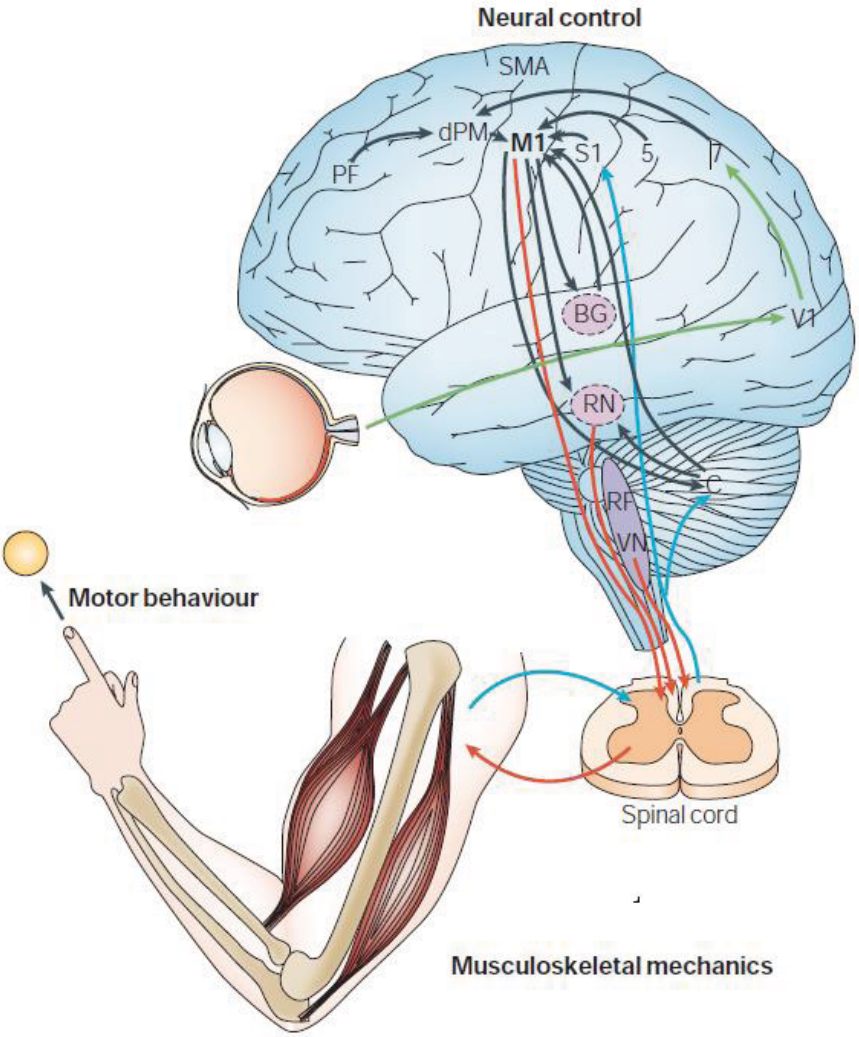

Figure 1-4. Brain areas involved in goal-directed movements (Scott, 2004). To achieve goal-directed movements, visual information is delivered through primary visual cortex (V1) and posterior parietal cortex (PPC). Sensory feedback is also transmitted by primary sensory cortex (S1). PM and SMA plan movements and M1 executes the movements. Basal ganglia (BG) and cerebellum (CB) are also involved in motor control through interaction with other motor related area.

1.2. Basic of Machine Learning

Machine learning is an essential algorithm to develop the BMIs. Algorithm of machine learning can be categorized into supervised learning, unsupervised learning, and reinforcement learning (Murphy, 2012).

In the **supervised learning**, the algorithm learns the relationship between inputs and outputs. During the learning labeled outputs are given to build a model of the relationship. After the learning, new inputs will be given and the algorithm predicts the outputs using the model.

In the **unsupervised learning**, unlabeled outputs are given to build the model unlike supervised learning. Because the algorithm does not know the collect answer, it clusters the data or finds similar patterns.

Reinforcement learning gives reward or penalty to the algorithm to indicate the desirability according to the action. Therefore algorithm can learn optimal actions to achieve the goals.

I will introduce more about the supervised learning. The algorithm involves two methods: **classification** and **regression** (Murphy, 2012). I will explain a classification method. The supervised learning has two step: **training** and **testing**. In the training step, labeled data is given to build the model as previously mentioned. During the training, the algorithm builds a model that describes the relationship between inputs and outputs. In testing step, the algorithm predicts the outputs from unlabeled new inputs based on the model. The training data can be camera images, sound signals, or

bio signals. The original data contains noises such as background image, ambient noise, or movement artifacts. Therefore, elimination of the noise is required. The process is called **preprocessing** (Fig. 1-5). After the noise reduction, the algorithm should find features to classify different classes. This is a process of **feature extraction**. Shape, size, or color of the objects can be used as features. Selection of features is very important in classification performance. Although many features can be used, it does not ensure the increase of the accuracy. The processes of preprocessing and feature extraction are same in training and testing step. Whereas, the algorithm builds a classifier during training step and classifies the new data during testing step. This is a process of **classification**. There are two types of classification algorithm: linear classifier and non-linear classifier (Fig 1-6). Although non-linear classifier shows good performance with training data, caution is required. Because the increase of non-linearity can cause error (over fitting).

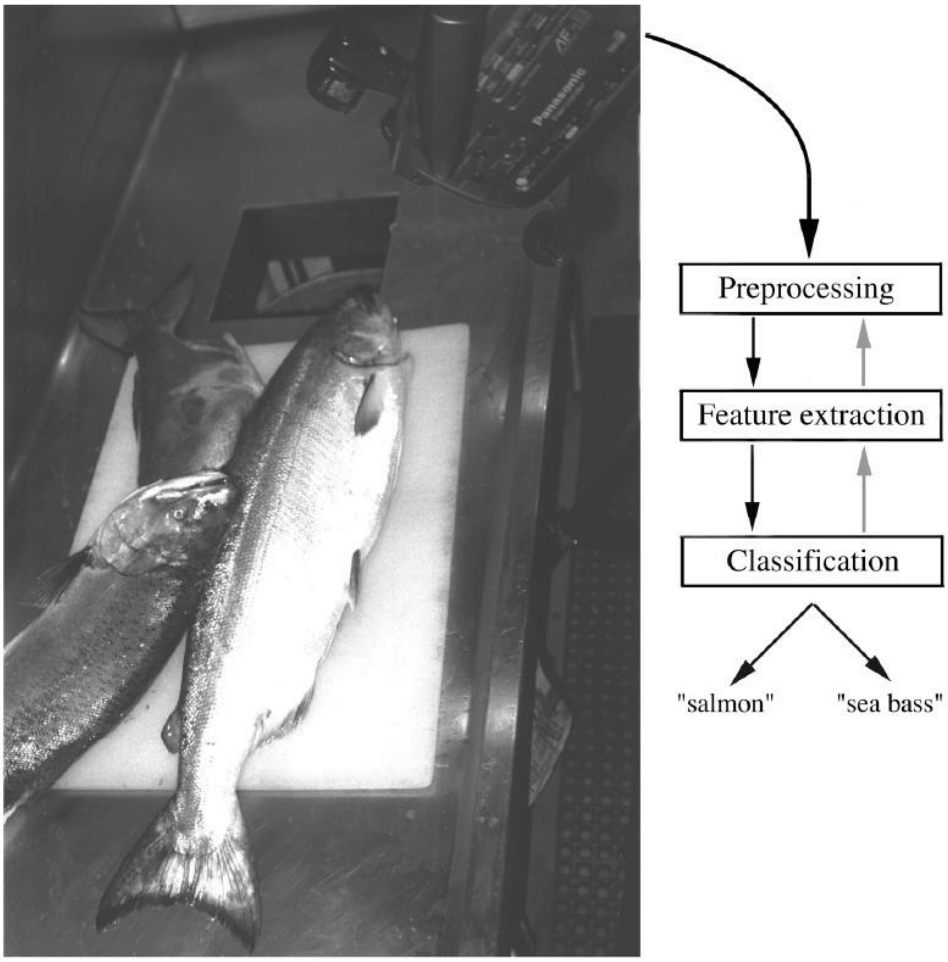

Figure 1-5. The process of classification (Duda et al., 2001). After the acquisition of data, preprocessing, feature extraction and classification are processed. The preprocessing removes noises such as background image, ambient noise, or movement artifacts. Shape, size, or color of the objects can be used as features.

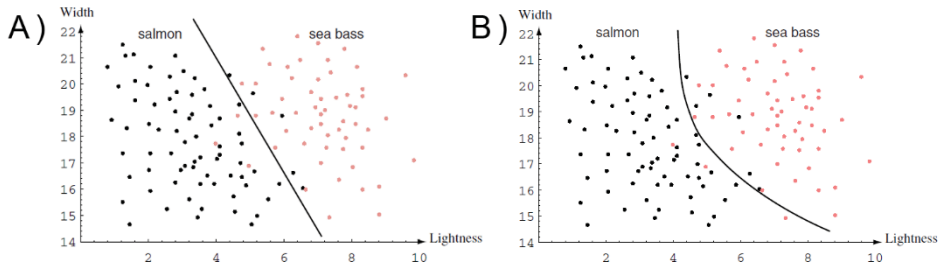

Figure 1-6. Two types of classification algorithm. a) Linear classifier. b) Non-linear classifier. Although non-linear classifier shows good performance with training data, caution is required. Because the increase of non-linearity can cause error (over fitting).

1.3. Brain-Machine Interface

Many people experience tremendous inconvenience in their daily life because of severe motor impairment caused by diverse conditions, including amyotrophic lateral sclerosis, spinal cord injury, stroke and cerebral palsy. The BMI is a promising technology that will help these disabled people to interact with the external world (Lebedev and Nicolelis, 2006, Dornhege, 2007, Wolpaw and Wolpaw, 2012). The brain sends a motor command to the muscle through spinal cord. People with a trouble in the pathway between the brain and muscles cannot move their body, although the brain can send a command. The BMI measures the brain signals and recognizes the user's intention to control external devices instead of a spinal cord and muscles. Here, I will briefly introduce basic knowledge about the BMIs.

1.3.1. Methods to Measure the Brain Signals

The methods to measure the brain signal are divided into **invasive** and **non-invasive** method (Fig. 1-7). Invasive recording provides informative signals (high signal to ratio). Therefore, it is a very useful method for helping people with severe motor disabilities. However, invasive method can cause a damage to the brain tissue and the method is unstable for long-term recording (Ince et al., 2010). Whereas a non-invasive method can provide a convenient interface to less severely disabled patients or healthy people, without a need for surgery.

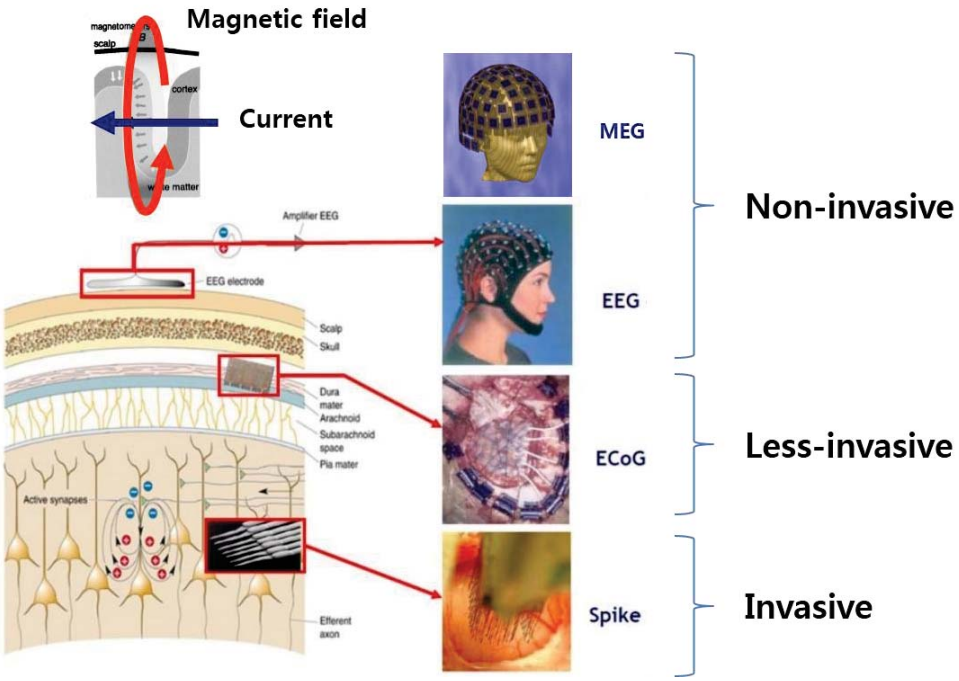

Figure 1-7. The methods to measure the brain signal. The methods are divided into invasive and non-invasive method. Invasive recording provides informative signals. However, a non-invasive method can provide a convenient interface to less severely disabled patients or healthy people, without a need for surgery.

1.3.2. Process of the BMIs

Process of the BMIs consists of signal **acquisition**, **preprocessing**, **feature extraction**, **prediction** and control of device (Fig. 1-8). It is similar with the signal processing for classification previously mentioned in section 1.2. Preprocessing is a process to reduce noise such as re-referencing, band-pass filtering and independent

component analysis (ICA) for artifact removal. Basically line noise is removed using notch filter (60Hz in Korea) and common average reference (CAR) is applied for electroencephalography (EEG) signals. Feature extraction reduces the amount of the data and extracts changes of brain signals related to user's intention. Features used in BMIs will be introduced in section 1.3.3. Prediction can be divided into classification and regression. Classification divides the intention into several categories such as left, right, front and back. Regression estimates continuous values such as movement velocity. Classification or regression is a process to predict the user's intention from the signal features. Finally, machine or computer is controlled according to the prediction results.

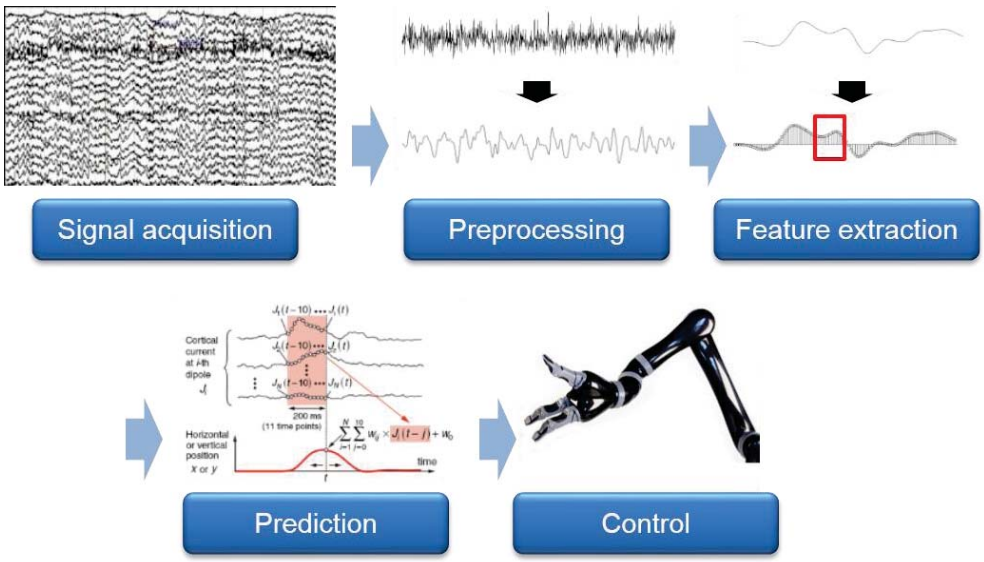

Figure 1-8. Process of the BMIs. It consists of signal acquisition, preprocessing, feature extraction, prediction and control of device. Preprocessing is a process to

reduce noise such as re-referencing, band-pass filtering and independent component analysis (ICA) for artifact removal. Feature extraction reduces the amount of the data and extracts changes of brain signals related to user's intention. Prediction can be divided into classification and regression. It is a process to predict the user's intention from the signal features. Finally, machine or computer is control according to the prediction results.

1.3.3. Different Methods of the BMIs

There are several different methods to predict user′s intention (Fig. 1-9). **Sensorimotor rhythms (SMR)** uses the increase or decrease of alpha or beta power on motor cortex to control the cursor to the left or right. The increase or decrease of signal power is called **event-related synchronization (ERS)** or **desynchronization (ERD)**, respectively. **P300** is a method finding P300 which has maximum amplitude when a subject watches a screen with flashing characters. Using the method, the subject can select a character by concentrating on the character. **Steady state visually evoked potential (SSVEP)** finds a target when a subject watches visual stimuli which is flashing at different frequency. Although SMR, P300 and SSVEP are useful methods, these are limited to select limited options. If a BMI user can control robotic arm like his/her arm, then unlimited things will be possible. **Directional tuning** is a property of some neurons on the M1 that the firing rate is highest in a preferred

direction and decreases gradually when the movement directions become far away from the preferred direction (Georgopoulos et al., 1982). Using the directional tuning, continuous movement trajectory can be predicted (Hochberg et al., 2012, Collinger et al., 2013, Yeom et al., 2013).

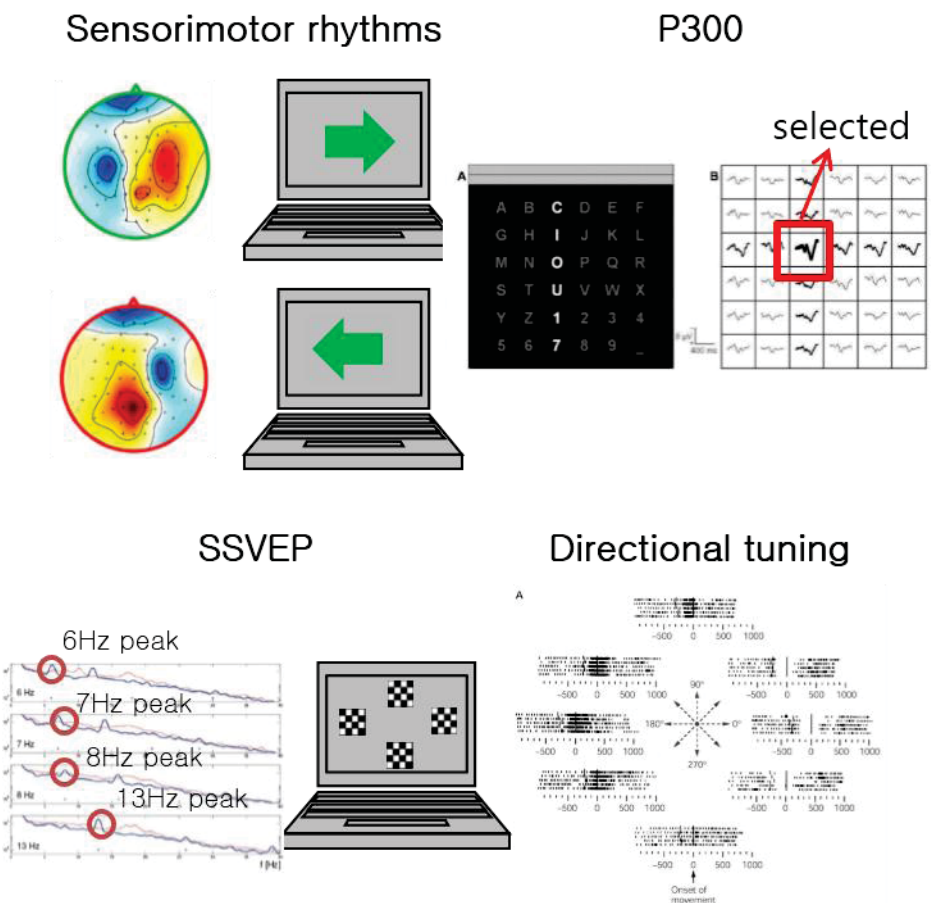

Figure 1-9. Several different methods to predict user's intention. Sensorimotor rhythms (SMR) uses the increase or decrease of alpha or beta power on motor cortex to control the cursor left or right. P300 is a method to detect a character by finding

P300 which has maximum amplitude. Steady state visually evoked potential (SSVEP) finds a target when a subject watches visual stimuli which is flashing at different frequency. Although it is useful, previous BMI methods are limited to select limited options. If a BMI user can control robotic arm like his/her arm, then unlimited things will be possible.

Chapter 2: Movement Trajectory Prediction

2.1. Introduction

Over the last several decades, monkey and human studies have been performed to identify movement intentions from brain activity, which can be used to restore movement function. In 1982, Georgopoulos found that some neurons in the M1 have direction preference (Georgopoulos et al., 1982), as I previously mentioned in section 1.3.3. That author also demonstrated that movement direction can be inferred from a vector sum of weighted preferred directions (Georgopoulos et al., 1986). Since then, the many invasive BMI studies performed on monkeys and humans revealed that arm movements can be estimated from spiking activity (Wessberg et al., 2000, Taylor et al., 2002, Santhanam et al., 2006) and local field potentials (LFPs) (Ince et al., 2010; Flint et al., 2012) in monkeys, and from spiking activity (Hochberg et al., 2006; Chadwick et al., 2011; Simeral et al., 2011) and electrocorticography (ECoG) (Schalk et al., 2007; Pistohl et al., 2008; Milekovic et al., 2012) in humans. Moreover, monkeys can feed themselves by controlling a robotic arm as if it were their own arm in real time (Velliste et al., 2008), and each finger and joint movement can be inferred from brain activity (Vargas-Irwin et al., 2010). More recent study also demonstrated that people with tetraplegia can drink coffee by controlling a robotic arm via neural activity recorded from microelectrode arrays (Hochberg et al., 2012).

Invasive recording provides informative signals; therefore, it is a useful method for

helping people with severe motor disabilities. However, invasive method can cause a damage to the brain tissue and the method is unstable for long-term recording. Whereas, a non-invasive method can provide a convenient interface to less severely disabled patients or healthy people, without a need for surgery. Therefore, non-invasive BMI studies estimating movement intentions are also required for convenient and general use. To control prosthetic devices, brain signals need to be translated into 3-dimensional control signals. However, the development of non-invasive interfaces for the estimation of 3-dimensional movements is at a very early stage.

To the best of our knowledge, only one study has used a non-invasive approach to estimate three-dimensional movements. That study reported results of the reconstruction of three-dimensional movement trajectories using electroencephalography (EEG) signals (Bradberry et al., 2010). Those results are important and meaningful in that they demonstrated the potential for estimating three-dimensional movements using a non-invasive interface. However, the correlation coefficients of the study were not high (mean r = 0.19–0.38) and it was not obvious whether the trajectories varied depending on the original movements or they varied periodically irrespective of the original movement, because the movement intervals were very short. One of the plausible explanations for the low accuracy of that method is that the authors used EEG signals that were low-pass filtered at 1 Hz for movement decoding. However, movement-evoked potentials (MEPs) during arm movements include components that are faster than 1 Hz (Rickert et al., 2005). Therefore, their results might not fully reflect the characteristics of MEPs.

Here, I aimed to estimate 3-dimensional movements based on non-invasive brain signals filtered with a frequency band that includes the characteristic frequency range of MEPs during arm movements (Yeom et al., 2013). A whole-head magnetoencephalography (MEG) system and a 3-axis accelerometer were used to measure brain activities and finger velocities. Sixty-eight MEG channels in motor-related areas were selected for movement decoding. The signals of the channels were band-pass filtered using 4 subfrequency bands and the filtered signals were resampled. I applied a multiple linear regression (MLR) algorithm to estimate movements from the MEG signals, and mean correlation coefficients were calculated to evaluate the decoding accuracy.

2.2. Methods

2.2.1. Experimental Procedure

Nine right-handed subjects who were not color-blind (age, 19–37 years, 5 men and 4 women) participated in this experiment. The score on the Edinburgh Handedness Inventory was above 80 in all subjects (Oldfield, 1971). The experiment was approved by the Institutional Review Board of the Seoul National University Hospital. During the experiment, each subject was instructed to move his/her right arm only in a specified 3-dimensional space without any other movements. To instruct 3-dimensional movements, stereographic images were presented on a screen using a STIM2 system (Neuroscan, El Paso, TX, USA) (Fig. 2-1(A), (B)). At the beginning of the experiment, a sphere was presented on the center of the screen for 4 s, and the subject was asked to put his/her index finger on the sphere. After 4 s, a target sphere with a stick connecting it to the center sphere appeared on one corner for 1 s. During this time, the subject was instructed to move his/her index finger from the center to the target on one corner and come back to the center along the stick line (center-out paradigm). The target sphere was presented randomly on each of the 4 corners (upper-left, upper-right, bottom-left, and bottom-right corners). This sequence was repeated during the session (Fig. 2-1C). One session of the experiment consisted of 30 trials for each direction (total, 120 trials). For each subject, 2 sessions were measured. During the experiment, a cushion was placed under the subject's elbow to minimize

movement artifacts and to make him/her more comfortable (Fig. 2-1A).

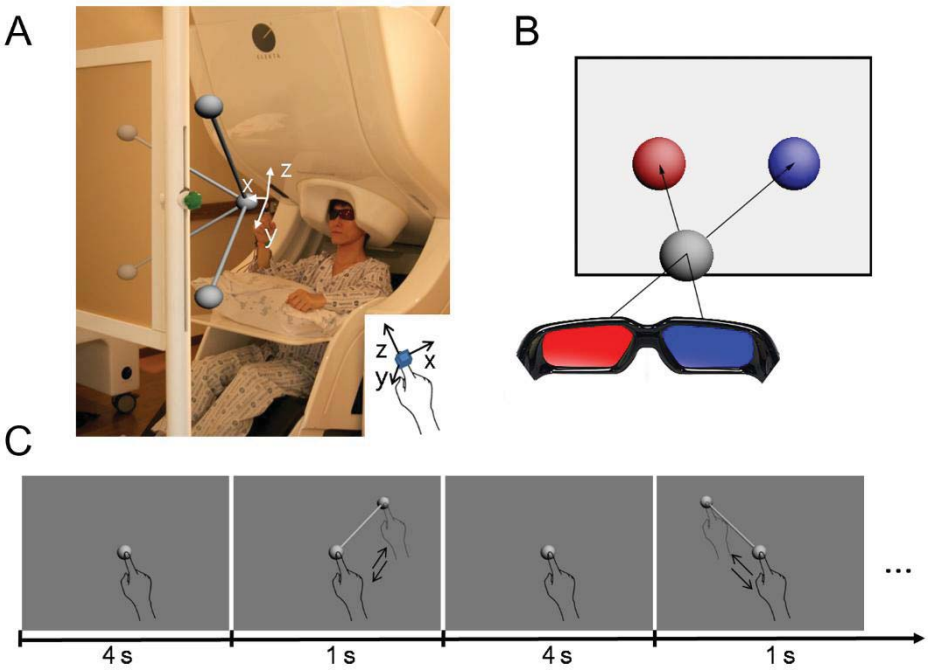

Figure 2-1. Experiment paradigm. (A) A photograph showing the visual stimuli and the coordinates of the accelerometer. The direction to the right side from the index finger was the x-axis, the direction down from the finger was the y-axis, and the direction to the end point was the z-axis. The coordinates can vary slightly among subjects because of their somewhat different postures. A cushion was placed under the subject's elbow to minimize vibration. (B) Principle of the anaglyph. The subject feels that the object exists at the intersection point. (C) Drawings show the sequence of visual stimuli and instructed behaviors.

2.2.2. Stereographic Images

I applied an anaglyph approach to generate 3-dimensional stimulus images. The principle of the anaglyph is as follows. When a subject looks at an image wearing colored glasses, he/she cannot see an image of the same color. Thus, the eye that is covered with a red glass can see the blue image only, and the other eye, covered with a blue glass, can see the red image only. Thus, the images overlap at the intersection and the subject senses that an object exists at the intersection point (Fig. 2-1B). I used the Autodesk 3ds Max 2011 program (Autodesk, San Rafael, CA, USA) to generate images with different views, because 2 images of the same object viewed from different angles are needed to generate an anaglyph image. Subsequently, these images were transformed into anaglyph images using the Anaglyph Maker Ver. 1.08 software, which is available at http://www.stereoeye.jp.

2.2.3. Data Acquisition

The MEG signals were measured using a 306-channel whole-head MEG system (VectorView TM, Elekta Neuromag Oy, Helsinki, Finland), which has 306 sensors in triplets consisting of 2 planar gradiometers and 1 magnetometer distributed at 102 locations that form a helmet shape. All measurements were conducted in a magnetically shielded room. I only used gradiometers for analysis and decoding because of their greater signal-to-noise ratio (SNR) compared with magnetometers

(Hamalainen et al., 1993). The sampling frequency was 600.615 Hz and the signals were filtered using a band-pass filter in the range of 0.1–200 Hz. A 3-axis accelerometer (KXM52, Kionix, NY, USA) was used to record movement trajectories. The accelerometer was placed on the index finger and the sensor signals were recorded simultaneously with the MEG signals using the same sampling frequency.

2.2.4. Preprocessing

To increase the SNR of the MEG signals, the spatiotemporal signal space separation (tSSS) method was applied, as it eliminates the external interference signals (Taulu and Simola, 2006). All data processing was performed using MATLAB 2008b (Mathworks, Natick, MA, USA). The MEG signals were segmented into a series of epochs each from -1 to 2 seconds before target onset and band-pass filtered at 0.1–100 Hz. Accelerometer signals for x-, y-, and z-axes were filtered with a band pass of 0.2–5 Hz and the linear trends were removed. The velocities of the index finger were calculated by integrating the accelerometer signals.

2.2.5. Time-Resolved Power Spectra

Time-resolved power spectra were calculated for each subject for all trials on 204 whole-head gradiometer channels with a continuous wavelet transform (CWT) at a frequency resolution of 1 Hz. The baseline of the power spectra was from −1 s to 0 s

from the cue onset. Each frequency power spectrum was normalized to each baseline frequency bin to identify the power spectrum changes for each frequency bin (Rickert et al., 2005). The power spectra were normalized and averaged across subjects. For the analysis, the 204 gradiometers placed at 102 locations were used and the time-resolved power spectra for the latitudinal gradiometer and longitudinal gradiometer at the same location were averaged. Thus, 102 time-resolved power spectra were presented for 204 gradiometer channels. Fig. 2-2A shows the time-resolved power spectra averaged across all subjects and all trials on whole-head gradiometer channels. These 68 gradiometer channels at 34 locations (surrounded by the black line in Fig. 2-2A) were selected for movement decoding. Power spectra of channels within the black line had an ERD around alpha (8–13 Hz) and beta (13–30 Hz) frequencies that are prominent in motor-related areas (Fig. 2-2A) (Pfurtscheller and da Silva, 1999). Fig. 2-2A depicts the time-resolved power spectrum marked with a red rectangle in Fig. 2-2A, which exhibited clear ERD and ERS. ERS occurred at 0.5–8 Hz and 57–98 Hz, whereas ERD appeared at 9–22 Hz (Fig. 2-2B). At 25–40 Hz, ERD was changed to ERS after the movements. I determined the subfrequency band for decoding based on these results.

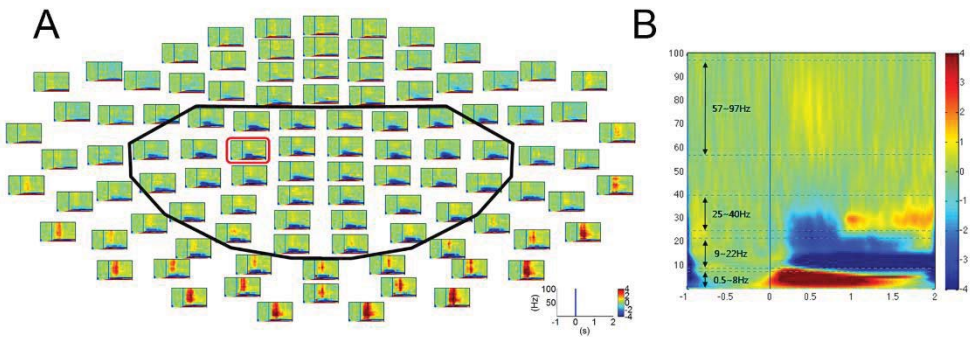

Figure 2-2. Brain activity modulation during movements. (A) Normalized time-resolved power spectra averaged across all subjects and all trials on 204 whole-head gradiometer channels. A CWT was applied at a frequency resolution of 1 Hz. The baseline of the power spectrum was from 1 s before to 0 s after the cue onset. The time-resolved power spectra of latitudinal and longitudinal gradiometers were averaged. (B) Normalized time-resolved power spectrum averaged across all subjects and all trials on a single gradiometer channel, which is marked with a red rectangle in Fig. 2-2A.

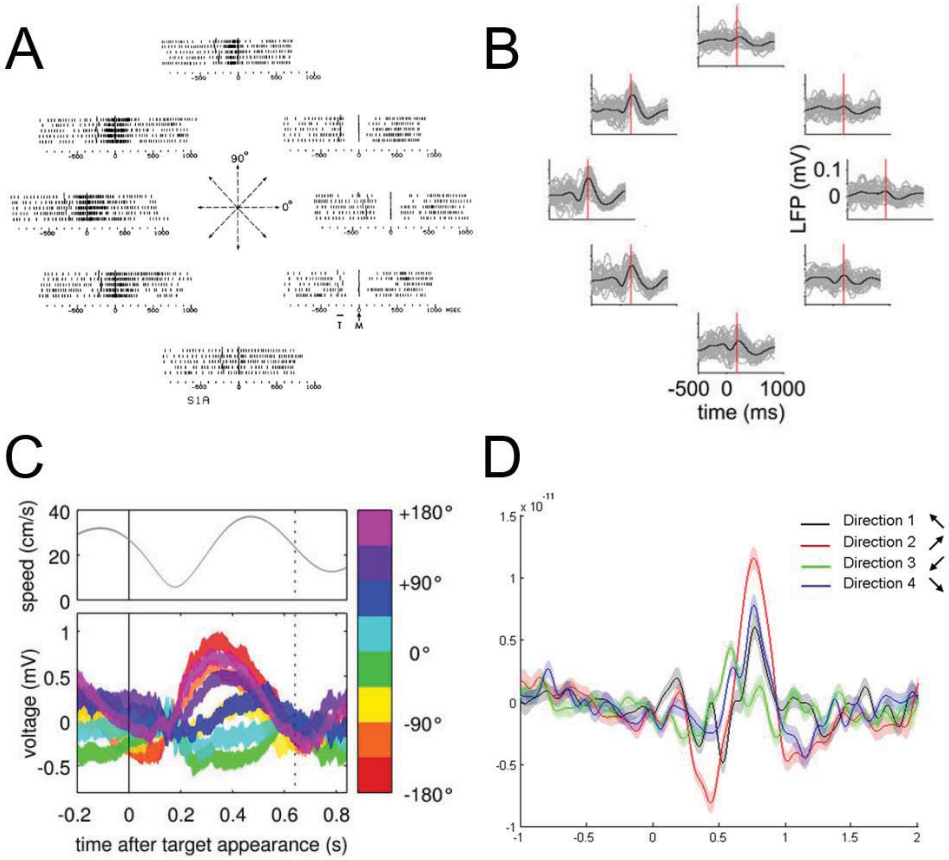

Figure 2-3. Directional tuning in different types of neural signals. (A) Spike activities measured from monkey during center-out movements (taken from (Georgopoulos et al., 1982)). (B) Trial-averaged (black) and single-trial (gray) LFP signals of monkey during center-out movements (taken from (Waldert et al., 2009)). (C) Human ECoG signals from one electrode on hand/arm motor cortex for eight directions (taken from (Waldert et al., 2009)). (D) MEG signal patterns that were band-pass filtered at 0.5–8 Hz and the standard error of the mean (SEM) for 4 different direction movements on the same channel (marked by a red rectangle in Fig. 2-2A).

2.2.6. Decoding

The 68 gradiometer channels selected may include motor-related areas (Waldert et al., 2008). Signals from the 68 channels were band-pass filtered using 4 subfrequency bands (0.5–8, 9–22, 25–40, and 57–97 Hz). I examined whether movement velocities can be inferred from signals from each frequency band. The 4 subfrequency bands were determined based on the time-frequency analysis (Fig. 2-2B) and approximately corresponded to delta and theta (0.5–8 Hz), alpha and low beta (9–22 Hz), high beta (25–40 Hz), and gamma (57–97 Hz) frequencies. The signals filtered into 0.5–8 Hz and 9–22 Hz bands were resampled at an interval of 20 ms and the current time point plus its 10 preceding time points (for a total of 11 points) corresponding to a 200 ms interval were used to estimate the current movement velocity (Toda et al., 2011). Likewise, the signals filtered into 25–40 and 57–97 Hz bands were resampled at intervals of 10 and 5 ms to preserve their characteristics based on the sampling theorem (Shannon, 1949). In addition, the 11 points corresponding to the preceding 100 ms and 50 ms intervals from the current time t were used for estimations of current movement velocities. In all cases, these 11 points of 68 channels (for a total of 748 points) were used as features, and the x, y, and z velocities of the movements were estimated using a MLR method, as follows;

$$x(t) = \sum_{i=1}^{n} \sum_{j=0}^{m} W_{ij}^{x} \times S_i(t-j) + W_0^x$$

$$y(t) = \sum_{i=1}^{n} \sum_{j=0}^{m} W_{ij}^{y} \times S_i(t-j) + W_0^{y}$$

$$z(t) = \sum_{i=1}^{n} \sum_{j=0}^{m} W_{ij}^{z} \times S_i(t-j) + W_0^{z}$$

where x(t), y(t), and z(t) are estimated movement velocities at time t; W_{ij}^{x}, W_{ij}^{y}, and W_{ij}^{z} are weight value matrices obtained from the regression methods and S_i is a MEG signal of channel *i*; *n* is the number of channels (68 in this study); *m* is the number of data points before time *t*, which determines the number of past data points that were used to estimate the current velocities x(*t*), y(*t*), and z(*t*). Although the results were illustrated at an m value of 10, I compared the averaged correlation coefficients across subjects, trials, and axes by changing data point number *m*, to investigate the effects of past brain activity; *j* is the time lag; and W_0 is the constant used to compensate for errors. W_{ij} and W_0 were obtained by training using the MLR.

2.2.7. Evaluation

A 5-fold cross validation was applied to assess the accuracy of the decoding. This method separates the data into four-fifths for training and one-fifth for testing (Fruitet et al., 2010). Thus, 5 combinations of training and testing data were available. Parameters of the MLR were obtained using the training data, and the accuracy of the estimations was evaluated using the testing data by calculating Pearson's correlation coefficients (*r*) between the real and estimated movement trajectories for each cross-

validation fold. The correlation coefficients were averaged across the cross-validation folds and sessions.

2.2.8. Trajectory of hand movements

To visualize the trajectories of hand movements, positions were also calculated by integrating the real and estimated velocities. Because the accelerometer measured relative displacement, but not absolute coordinates, measurement errors of the accelerometer signals accumulated during the integration. Therefore, the starting positions of trials were not identical, even though the signals were band-pass filtered and linear trends were removed to compensate for the measurement errors. For this reason, I illustrated the trajectories only during movements and the starting positions were set to zero when visualizing the results in Figs 4 and 5a, b. The visualized duration of each movement was determined individually (mean ± SD, 307.6 ± 114.3 ms to 1,200.9 ± 292.2 ms from the cue onset).

2.2.9. Topographic maps of weight values

The magnitude of the weights obtained from the regression algorithm represents the importance of the features in the estimation of movement (Bradberry et al., 2010; Chan et al., 2011). To examine the contributions of the features to estimations, I projected the weights onto topographic maps using the topoplot function of EEGLAB

10.2.2.4a (Delorme and Makeig, 2004) at each time point. For this, the absolute values of weight matrices were calculated and averaged across folds, axes, subjects, and channels at a same location. As a result, I obtained weights for 34 locations at 11 time points. Because channels that were not used for estimation did not have weight values, those were set to zero. Averaged absolute weights are color coded on the scalp map and the channels used for decoding are indicated by black dots (Fig. 2-7).

2.3. Results

Movement velocities were estimated using the low-frequency MEG signals (0.5–8 Hz), whereas the other 3 frequency band signals could not decode these velocities. Therefore, I focused on the results of estimations based on the low-frequency activity and did not display the results from the other frequency bands. The amplitudes of signals filtered at 0.5–8 Hz varied according to different direction movements. Fig. 2-3D illustrates a sample result that was derived from 1 subject during 1 session using a single channel (marked by a red rectangle in Fig. 2-2A). The lines depict average signals across trials and the colored shadow lines indicate the SEM.

Previous studies reported that not only spikes but also low-pass-filtered movement-related potentials (MRPs) of LFP and ECoG are directionally tuned (Fig. 2-3) (Rickert et al., 2005; Waldert et al., 2008; Waldert et al., 2009). My results verify that changes of neural activities are also measurable with a non-invasive method.

I evaluated the significance of the results by calculating Pearson's correlation coefficients (r); the mean correlation coefficients with standard deviations are plotted in Fig. 2-4A. All correlation coefficients were significant ($p < 0.001$). The mean correlation coefficients on the x-axis, y-axis, and z-axis averaged across the 9 subjects were 0.670 ± 0.056, 0.697 ± 0.041, and 0.749 ± 0.046, respectively. These correlation coefficients were considerably high, although the correlation coefficients of subject 2 were relatively low. A plausible explanation for the low accuracy obtained for this subject is offered in the Discussion.

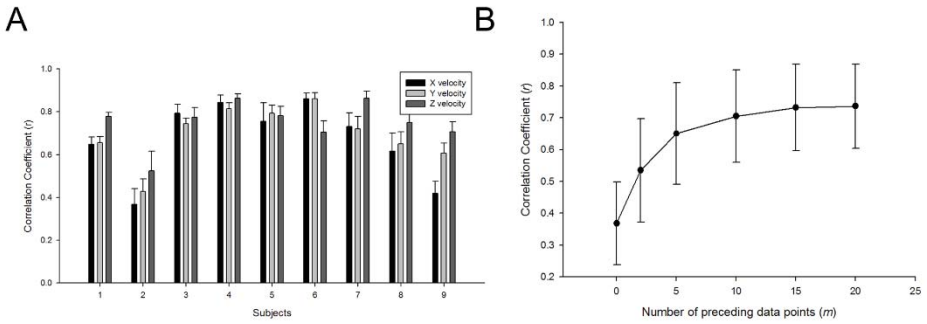

Figure 2-4. Correlation coefficients. (A) Averaged Pearson's correlation coefficients (r) between real and estimated movement trajectories with standard deviations across cross-validation folds and for all sessions. (B) The correlation coefficients averaged across all subjects, trials, and axes increased gradually according to the increase in the number of preceding data points (*m*).

Fig. 2-4B shows the number of preceding data points (*m*) required to estimate the current velocity. When *m* was zero, which meant that only the current MEG signal amplitudes were used, the correlation coefficient averaged across subjects, trials, and axes was 0.369 ± 0.130. The correlation coefficients increased according to the increase of *m*. However, the increase in the correlation coefficients was gradually saturated. It seemed that 10–15 data points were sufficient to estimate most of the movements in the case of the MEG signals, which were resampled at 20 ms. The correlation coefficients were 0.535 ± 0.162, 0.651 ± 0.159, 0.706 ± 0.145, 0.732 ± 0.136, and 0.737 ± 0.133 for *m* values of 2, 5, 10, 15, and 20, respectively.

Moreover, I visually confirmed the results of the movement estimations in 3-dimensional space. The mean values and standard deviations of the estimated movement trajectories across all trials for each subject are displayed in Fig. 2-5. These data indicate that the estimated trajectories were well discriminated for different directional movements in most of the subjects. Because I calculated the position by integrating the accelerometer signals twice and because some preprocessing was performed, the scale of axes was arbitrary.

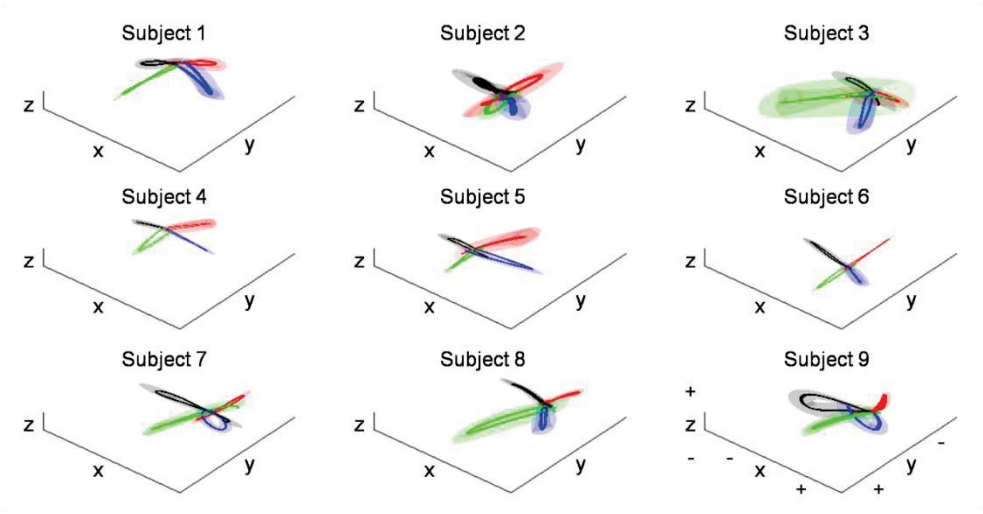

Figure 2-5. Averaged results of the estimation of movement trajectories across all trials for each subject. Shaded areas represent the standard deviation along averaged trajectories. Each color indicates one of four different directions. Black, red, green and blue represent up-left, up-right, down-left and down-right trajectories, respectively. The x-, y- and z-axes represent recording coordinates (see Fig. 1-1(A)). The scales of axes were arbitrary.

Single-trial-based estimation results also closely followed the real movements. Fig. 2-6A illustrates a real movement trajectory for 1 subject and Fig. 2-6B shows the results estimated from the MEG signals, as described in the “Decoding” and “Trajectory of hand movement” sections. Each line depicts a single-trial movement. Fig. 2-6C depicts sample results of real movements and estimated movements on the x-, y-, and z-axes. These results revealed that the estimated trajectory closely depicted the real movement trajectory, not only on each axis but also in a 3-dimensional space.

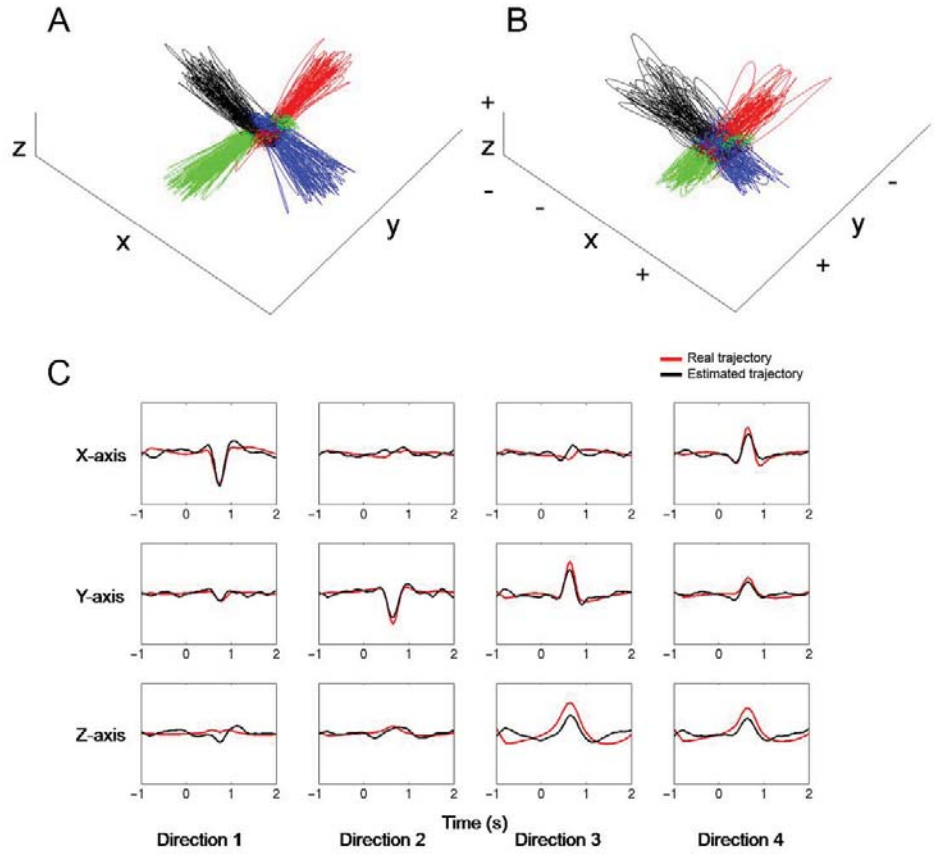

Figure 2-6. Single-trial-based estimation results. (A) Real movement trajectory for 1 session including 1 subject. (B) Movement trajectory estimated from the MEG signals. (C) Sample results of estimation of movement on the x-, y-, and z-axis for each direction.

The topography of weights revealed contributions of each channel and each time point to movement estimations (Fig. 2-7). The magnitudes of absolute weights increased until −100 ms and decreased thereafter. It seemed that brain signals recorded from −140 ms to −60 ms on the central regions were important for estimating the current velocity, which exhibited high-weight values.

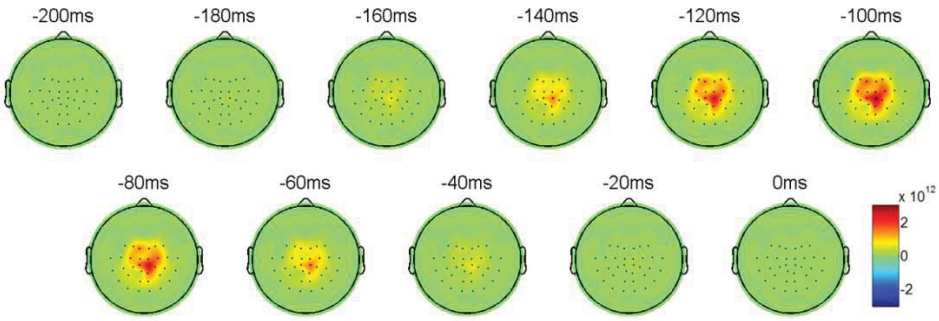

Figure 2-7. Temporal topographic maps of weight values. Each topographic map illustrates the weight values for previous brain activity that were used to estimate current fingertip velocity. The colors represent the magnitudes of averaged absolute weight values on the scalp maps. These results showed that brain signals recorded from −60 ms to −140 ms on the central regions had high weight values. The black dots depict the locations of the channels used for decoding movements.

2.4. Discussion

I demonstrated that non-invasive MEG signals can be used to estimate 3-dimensional reaching movements with considerably high performance. Moreover, the results revealed that low-frequency activity plays an important role in estimating 3-dimensional movements using a non-invasive method. In addition, I showed that MEG signals from −60 to −140 ms are important, and that 200–300 ms intervals are appropriate, for movement estimations. Furthermore, my method of movement estimation seems appropriate for most people. These results imply that disabled people will be able to control prosthetic devices without surgery in the near future and that the technology will support them in living without the help of others.

2.4.1. The Non-Invasive Method Is Sufficient to Estimate 3-Dimensional Movements

It is generally thought that signals measured using non-invasive methods are not sufficient to estimate complex and elaborate movements because of their low level of informativeness (Lebedev and Nicolelis, 2006). However, I demonstrated that non-invasive signals can be used to estimate 3-dimensional reaching movements with considerably high accuracy (mean $r > 0.7$). This might have been possible because of the strength of non-invasive methods measuring broader brain areas, although the SNR is somewhat lower than that of invasive methods.

Diverse brain areas are involved in skilled movements, such as reaching and grasping, because they require generating potential action plans, choosing among them, and translating the plan into a detailed motor command (Cui and Andersen, 2011). Specifically, the M1 is more relevant to musculoskeletal control (Graziano et al., 2004; Truccolo et al., 2008). The PM and SMA are involved in motor planning and preparation (Chen et al., 2010; Hoshi and Tanji, 2000; Tanji and Shima, 1994; Townsend et al., 2011). Moreover, some regions of the PPC, such as the parietal reach region, lateral intraparietal area, and dorsal area 5, are also very important for potential and selected motor plans (Cui and Andersen, 2007, 2011). Therefore, using brain activity from broad motor-related areas, such as the SMA, PMC, M1, and PPC, may yield better accuracy than using a small area of the M1. This perspective also corresponds to previous BMI studies, which revealed that movement could be predicted from multiple frontal and parietal cortical areas (Nicolelis and Lebedev, 2009). In this regard, non-invasive methods are beneficial because invasive approaches using a microelectrode array generally measure a very small area (typically 4 × 4 mm) (Hochberg et al., 2012; Hochberg et al., 2006; Kim et al., 2008).

2.4.2. The Importance of Low-Frequency Activity in the Estimation of 3-Dimensional Movements

In 1982, Georgopoulos et al. reported that the firing rates of neurons in the primary motor cortex are tuned according to the directions of arm movements. Directional

tuning was observed in most measurement types and the tuning curve approximately resembled a cosine function (Waldert et al., 2009). The cosine tuning curves are present in the low-pass-filtered signals and the relevance of low-frequency activity has been reported (Waldert et al., 2009). As described in the "Introduction" section, the previous EEG study that estimated 3-dimenional movements used low-frequency activity (< 1 Hz), which was lower than the MEP frequency observed during arm movements. Moreover, as the movement intervals used in that study were not sufficiently long, it is not clear whether the reconstructed time course was the real estimation of movement or was a mere fluctuation. Therefore, it was unclear whether 3-dimensional movements could be estimated from low-frequency activity measured non-invasively.

In the experiment, the interval between movements was 4 s, which was sufficient to segregate rest and movement states. This clarifies that the estimated trajectory followed the original movements and did not just vary periodically. To minimize the movement artifacts, I instructed subjects not to move body parts other than the right arm during experiments, and a cushion was placed under the subject's elbow to minimize vibration. Moreover, their head movements were restricted by placing the head in a fixed MEG helmet (Fig. 1-1A). Moreover, the tSSS filtering applied to the signals, as described in the "Materials & Methods" section, reduced artifacts from external sources.

Here, I showed that 3-dimensional movements could be estimated quite accurately based on non-invasive measurements of low-frequency brain activity (0.5−8 Hz),

whereas the other frequency bands used could not decode the movements. Although studies have reported that high-frequency LFPs (200−400 Hz) had the best decoding performance (Zhuang et al., 2010), low-frequency activity plays an important role in estimating 3-dimensional movements, not only in invasive but also in non-invasive methods.

2.4.3. Preceding (60−140 ms) Brain Signals Are Important and 200−300 ms Intervals Are Appropriate for Movement Prediction

Although previous studies used data preceding current time points to estimate movements (Toda et al., 2011), the importance of these data and its optimal parameters were not specifically examined. Here, topographic maps of weights revealed that brain signals recorded from −60 to −140 ms exhibited high values, which implies that the duration is important to estimate movement velocity (Fig. 2-7). Furthermore, the comparison of correlation coefficients performed by changing the number of preceding data points showed that 200−300 ms (10−15 time points) were sufficient to estimate movements, as the correlation coefficients became gradually saturated as the number of preceding data points increased (Fig. 2-4B). Therefore, the results imply that brain signals recorded from −60 to −140 ms are important, and that 200−300 ms intervals are sufficient, to estimate the current velocity of movements.

2.4.4. The Method Is Feasible in Most Subjects

The correlation coefficients between real movements and estimated signals were considerably high in most subjects (mean $r > 0.7$), which is even higher than the correlation coefficients obtained in the ECoG study (mean $r \leq 0.3–0.6$) (Pistohl et al., 2008). Despite the good results obtained for most subjects, the correlation coefficients described in Fig. 2-6 were especially low for subject 2. To ascertain the reason for this low accuracy, I examined the movement trajectory during behavioral tasks. Based on the movement data, I observed that the finger positions of subject 2 during the experiment were not accurate and that the end positions of the finger varied. Thus, the parameters of the regression algorithm could not be correctly obtained because the trials performed for the same movements were not sufficient. For a similar reason, subjects for whom highly accurate results were obtained exhibited accurate and consistent movements.

2.4.5. Limitations

Although the results exhibited high accuracy, the study had several limitations, which must be resolved before the implementation of a practical BMI system. In this study, brain activity was measured using MEG. Although MEG has better spatial resolution compared with EEG, the MEG device is not portable, requires a magnetically shielded room, and is expensive. Therefore, additional EEG studies are needed to extend the

results into practical EEG-based BMI systems that may be available in daily life. Moreover, the BMI system should have a closed-loop design and function in real time for practical use and should be able to be applied to people with paralysis, which is one of the most important functions of BMI systems. However, my system does not function in real time and I did not demonstrate the method using patients. Nevertheless, in this study, I applied a simple signal processing method to estimate movements, such as selecting channels in regions of interest, band-pass filtering, down sampling, and applying a general regression algorithm. Therefore, I expect that it will be possible to build a real-time BMI system without technical problems using the methods.

Lastly, the movement tasks used in the experiments were simple. For actual movements, such as eating food or drinking water, the BMI system should be able to control artificial limbs with greater variability. Although additional experiments are needed to demonstrate that complex movements can be inferred from brain activities, I expect positive results, as previous invasive BMI systems that can grasp arbitrary targets used principles similar to my methods (Shimoda et al., 2012; Hochberg et al., 2012; Velliste et al., 2008).

For these reasons, I am planning to develop a closed-loop real-time BMI system that can control a robotic arm more freely, such as changing movement directions and choosing targets, and to verify the BMI system using patients with paralysis.

Chapter 3: Prediction Compensation

3.1. Introduction

Recent BMI studies could predict arm movements and control robotic arm in real-time (Hochberg et al., 2012, Collinger et al., 2013). However, the accuracy grasping the target is quite low. Success rates of the study were 20.8% – 62.2% for reaching and grasping movements (Hochberg et al., 2012).

Although the robotic arm approximately reached a target, grasping movements were often failed because the robotic arm did not exactly reach an object. The movement prediction inaccuracy is a critical barrier to practical application (Judy, 2012).

Such inaccuracy problem could be overcome by using feedback information. Movement control is achieved from not only motor commands but also sensory feedback (Kandel, 2012). Animals and humans compensate their movement errors by the feedback such as the position information obtained from proprioception and vision. Therefore, feedback information should also be considered in BMI system for high-accuracy. However, feedback information has not been directly used to update movement prediction model in the previous BMI studies, although the closed-loop BMI system provides the visual feedback to users. Therefore, efforts and times for adaptation are required to BMI users.

Unfortunately, it is difficult to extract the sensory feedback from the neural activity. Instead, we can obtain useful information by adding a stereo camera to the BMI

system. For example, the positions of objects can be calculated from an image recorded by an external camera and movement prediction can be compensated toward the object position as a movement goal. The positions of objects can be easily calculated from the image by the image segmentation method, which is a conventional technique (Fig. 3-1; see (Haralick and Shapiro, 1985)).

Here, I propose a BMI framework combining image processing with a novel prediction method, the feedback-prediction algorithm (FPA) that generates feedback information from the positions of objects and modifies movement prediction with the feedback (Figs. 3-1, and 3-2) (Yeom et al., 2014). The FPA predicts a target among objects based on the movement direction predicted from the neural activity. After the target selection, the FPA modifies the predicted direction toward the target and modulates the magnitude of the predicted vector to easily reach the target (Fig. 3-2A). The FPA repeats the modification in every prediction time points. To evaluate the performance improvements provided by the feedback, I predicted 3-dimensional reaching movements from MEG signals in both cases with feedback (FPA) and without feedback and then compared the prediction accuracy.

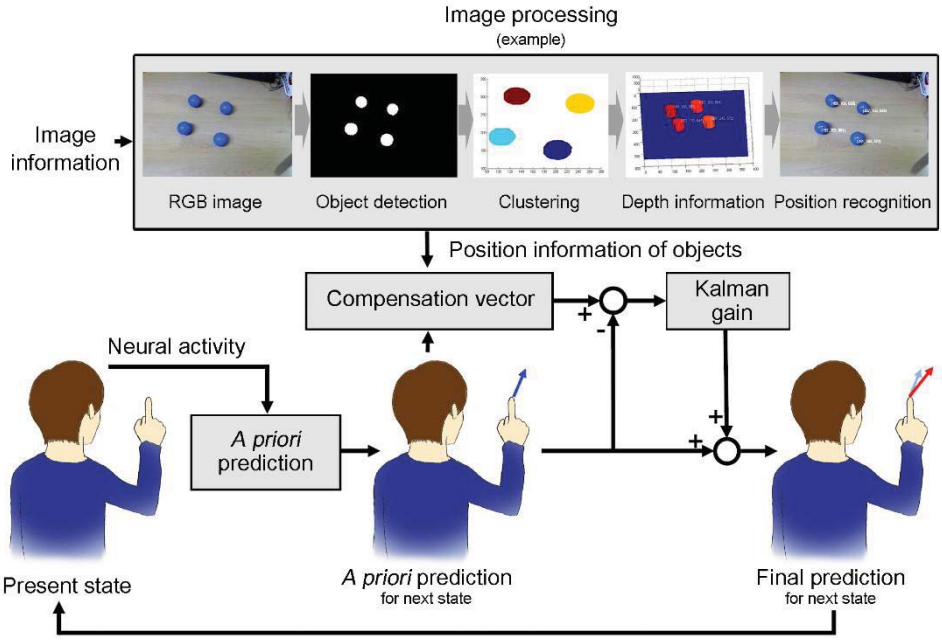

Figure 3-1. A BMI framework combining image processing. The BMI framework receives image information through external device. Position information of objects are calculated from the image information by image processing. The proposed FPA algorithm generates a compensation vector based on the position information and A priori prediction. The purpose of the compensation vector is to rotate the prediction vector toward the predicted target and magnify the predicted vector to easily reach the target. The FPA predicts the movement and compensates using the position information recursively.

3.2. Methods

3.2.1. Data Acquisition and Signal Processing

I used the same MEG data during center-out reaching movements describe in Chapter 2. For the movement prediction, I selected 68 gradiometer channels on motor-related areas based on power spectrum analysis. The MEG signals were band-pass filtered at 0.5−8Hz, and downsampled to 50Hz. Eleven data points preceding the current data point were used as features for predicting velocity. The movement velocities of x, y, and z were predicted from the regression method without feedback and with feedback (FPA). After the movement velocity prediction, the movement trajectories were calculated by integrating the predicted velocities.

Because the stereographic images were presented instead of real objects in my experiment, I assumed that object positions were equal to the mean position of the end points of real movement trajectory instead of the real image processing.

3.2.2. Feedback-Prediction Algorithm (FPA)

In previous BMI studies using a Kalman filter, the next state was usually predicted from the present state and the prediction was compensated based on the neural signals (Wu et al., 2004, Kim et al., 2008, Kim et al., 2011). Therefore, the method ensures that the prediction maintains the direction of the previous movements and it diminishes variation of prediction. This approach can be beneficial in the case of the prediction for smooth movements. However, the method may hinder the prediction of movement with rapid change. In robotics, the system generally estimates the next state from the present state with input signals and compensates the prediction based on measurement value, when measurement is possible (Thrun et al., 2005). Therefore, it is more reasonable to predict the next state from the present state with neural activity and compensate the prediction by the measurement such as with the proposed FPA.

The FPA is a recursive prediction algorithm consisting of three steps: 1) *a prior* prediction, 2) generation of a compensation vector, and 3) final prediction. In the *a prior* prediction step, the next movement state was predicted by the MLR from the previous movement state and the MEG signals. The *a prior* prediction method corresponds to the general prediction method used in various BMI studies (Velliste et al., 2008, Bradberry et al., 2009, Ganguly et al., 2009, Bradberry et al., 2010, Flint et al., 2012, Hauschild et al., 2012, Yeom et al., 2013). In the generation step of a compensation vector, a target is predicted among the objects based on the direction of the *a prior* prediction vector. After the target selection, a new vector directing target

from a present position is created. The magnitude of the vector is modified based on the probability that the predicted target is a real target by multiplying a weight value. This is a compensation vector which is used as feedback information. The weight value helps the movement prediction easily reach the target. Lastly, the final prediction is determined by adding the Kalman gain-multiplied error (the difference between the *a prior* prediction and the compensation vector), to the *a prior* prediction. The process of the FPA is as follows (Fig. 3-2A).

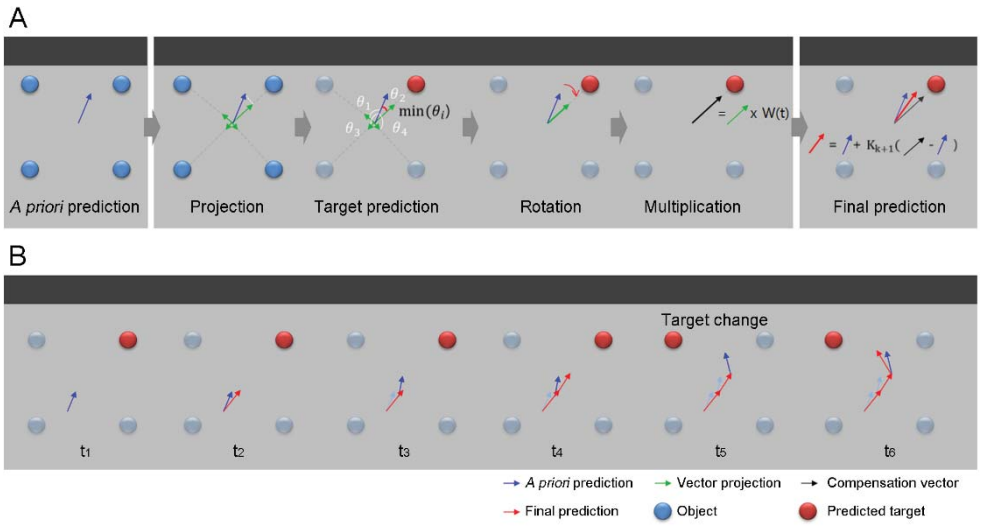

Figure 3-2. Principle of the FPA. (A) Three steps of the FPA. Step 1, the next movement state is a priori predicted from the present state and the neural activity. Step 2, the a priori predicted vector is projected onto the vectors directed from the present position to each object (green arrows are vector projections). One of the objects is predicted as the target which has the minimal angle between the predicted vector and vector projections (the red sphere). The predicted vector is rotated toward the target

and multiplied by a weight value (black arrow) to magnify the predicted vector to easily reach the target. Step 3, the final prediction vector (red arrow) is determined from a priori prediction and the compensation vector. (B) Prediction example while changing a target. The example shows how a target and final prediction can be changed according to the direction of a prior prediction.

Step 1. *A priori* prediction

In the first step, the next movement state was predicted from the previous movement state and the MEG signals. The relation between states, inputs, and measurements can be described with the state equation and output equation as follows:

$$x_{k+1} = Ax_k + Bu_k + w_k$$

$$y_k = Cx_k + z_k$$

where x_k is the state matrix (position) at time k; u_k indicates the MEG signal matrix; y_k is the measurement matrix which corresponds to a compensation vector; w_k describes the noise matrix and z_k is the measurement error matrix; *A*, *B*, and *C* are the coefficient matrices. In the study, I assumed that the matrix *A*, *C* is an identity matrix. *B* was calculated using the MLR.

To predict next *k*+1 state at time *k*, the FPA *a priori* predicts the next state of movements from the present state and neural activity as follows:

$$x_{k+1} = Ax_k + Bu_k$$

$$P_{k+1}^{-} = AP_k A^T + S_w$$

where x_{k+1} describes the *a priori* predicted next state and P_{k+1}^{-} is an *a priori* prediction error covariance and where S_w is a covariance matrix of system noise. I defined S_w as follows:

$$S_w = E(w_k w_k^T)$$

Step 2. Generation of a compensation vector

In the second step, a target is predicted among the objects and a compensation vector is generated. To predict a target, the *a priori* predicted vector is projected onto the vectors directed from the present position to each object.

$$Proj_{i;k+1} = x_{k+1} \cdot O_i = \left| x_{k+1} \right| \left| O_i \right| \cos\theta_i$$

where O_i is a unit vector pointing to each object i; θ_i is an angle between x_{k+1} and O_i. The length of the vector projection represents the degree of similarity of the predicted vector to the vector pointing to each object because the length of the vector projection is inversely proportional to the angle θ_i between the predicted vector and the vector directing the object. Therefore, an object corresponding to the maximal vector projection is predicted as the target as follows:

$$\text{Predicted\_target}_{i;k+1} = \arg\max_i \left\| Proj_{i;k+1} \right\| = \arg\min_i \theta_i$$

where $\left\| Proj_{i;k+1} \right\|$ is a Euclidean distance of the vector projection $Proj_{i;k+1}$. Because the target is predicted in every FPA process based on the neural activity, the subject can change his/her movement goal at any time (Fig. 3-2B).

After the target selection, the vector projection pointing to the target is multiplied by a weight value W(t). The purpose of multiplying the weight value is to help to easily reach the target. The weight value W(t) was calculated by dividing the length of

projection vector pointing to the target with the mean length of the projection vectors as follows:

$$W(t) = \frac{\left\| Proj_{target;k+1} \right\|}{\frac{1}{n}\sum_{i=1}^{n}\left\| Proj_{i;k+1} \right\|}$$

$$y_{k+1} = W(t) Proj_{target;k+1}$$

where y_{k+1} is the compensation vector. The weight $\mathrm{W(t)}$ was restricted to 2 to prevent overweight. I selected the appropriate restriction value by the experiment.

Step 3. Final prediction

In the final step, the final prediction vector is determined using the *a priori* prediction vector and a compensation vector calculated from the first and second steps. The *a priori* prediction x_{k+1} is compensated with the compensation vector y_{k+1} as follows:

$$K_{k+1} = AP_{k+1}^{-}C^{T}(CP_{k+1}^{-}C^{T} + S_{z})^{-1}$$

$$x_{k+1} = x_{k+1} + K_{k+1}(y_{k+1} - Cx_{k+1})$$

$$P_{k+1} = (I - K_{k+1}C)P_{k+1}^{-}$$

where K_{k+1} is called the Kalman gain and P_{k+1} is a *posteriori* prediction error covariance; the -1 superscript indicates the matrix inversion, the T superscript represents the matrix transposition; and S_z is a covariance matrix of the measurement error. I defined the S_z as follows:

$$S_z = E(z_k z_k^T)$$

I assumed that the S_w and the S_z were same and they were identity matrices in the study.

3.2.3. Evaluation of the Performance

I compared the performance in cases with feedback (FPA) and without feedback. To evaluate the performance, I assessed the closeness of the end points of the predicted trajectory to the target. I defined the error by the distances from the end point of the predicted trajectory to the target position, which was divided by the distance from the origin to the target position to normalize the error. In addition, movement error (ME) and movement variability (MV) were calculated (MacKenzie et al., 2001). ME represents an average distance of the predicted trajectory from the task axis. ME means how much a predicted trajectory is far from the ideal straight line. MV measures the standard deviation between a predicted trajectory and the task axis. MV depicts the variation of the predicted trajectory. For statistical analysis, I applied a paired-samples t-test to the errors in cases with feedback (FPA) and without feedback using SPSS, version 13.0 (SPSS, Chicago, IL).

3.3. Results

The results of the evaluation demonstrate that the end points of the trajectory predicted with the feedback were closer to the target and also more focused on the target than the end points predicted without feedback, because the magnitude and the direction of the predicted movement with feedback were modulated toward the target using the feedback information (Figs. 3-1, and 3-2).

The paired-samples t-test showed a significant group difference between errors in cases with and without feedback ($p < 0.001$), implying that the performance of the movement prediction was significantly improved by feedback (FPA). The mean error declined from 0.427 ± 0.238 to 0.290 ± 0.288 (mean ± SD) with feedback, corresponding to an error reduction of 32.1%. Because the reaching target was the virtual sphere, the variation of the real movements from the target center (error) was 0.178 ± 0.131. Based on the consideration of the real movement variation, the error of the FPA is considerably low. Fig. 3-3 illustrates the error bar and standard error in cases with feedback (gray) and without feedback (black) for each subject. I also evaluated the individual difference between errors in cases with feedback and without feedback by the paired-samples t-test. The p-values of most subjects were under 0.001 ($p = 0.021$ and $p = 0.002$ for subject 2 and subject 9, respectively).

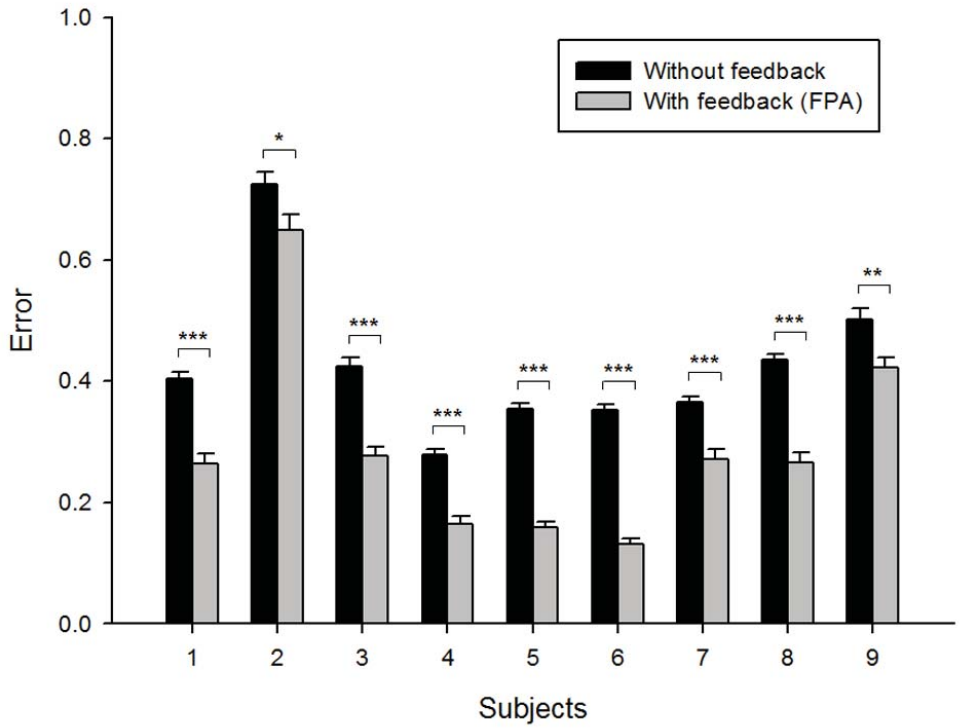

Figure 3-3. Error bar with standard error for each subject. Black bars illustrate errors in a case without feedback and gray bars represent errors in a case with feedback (FPA). *$p = 0.021$, **$p = 0.002$, ***$p < 0.001$

Moreover, ME and MV were significantly decreased by feedback ($p < 0.001$ and $p < 0.05$, respectively). The mean ME without feedback was 0.1146 ± 0.0722 and the mean ME with feedback was 0.0811 ± 0.0925. The mean MV without feedback was 0.0724 ± 0.0512 and the mean MV with feedback was 0.0698 ± 0.0850. The results

represent that predicted trajectories were closed to the optimal path and the variations of the predicted trajectories were reduced by feedback.

Note that the prediction results without feedback already showed high performance (mean $r > 0.7$) as described in my previous study (Yeom et al., 2013). Nevertheless, performance was significantly improved by combining the feedback information generated from the positions of objects.

Fig. 3-4 shows the example results of one subject during one session. Predicted movements without feedback roughly followed the original movements (Figs. 3-4B, and 3-4D). However, the predicted trajectory without feedback often did not reach the target. On the other hand, the predicted movements with feedback almost did reach the target (Figs. 3-4C, and 3-4D). Although real movements were somewhat scattered because the subject was instructed to reach to the virtual target, the predicted movement trajectory with feedback was more focused on the target because the predicted trajectory with feedback was compensated toward the target based on the target position.

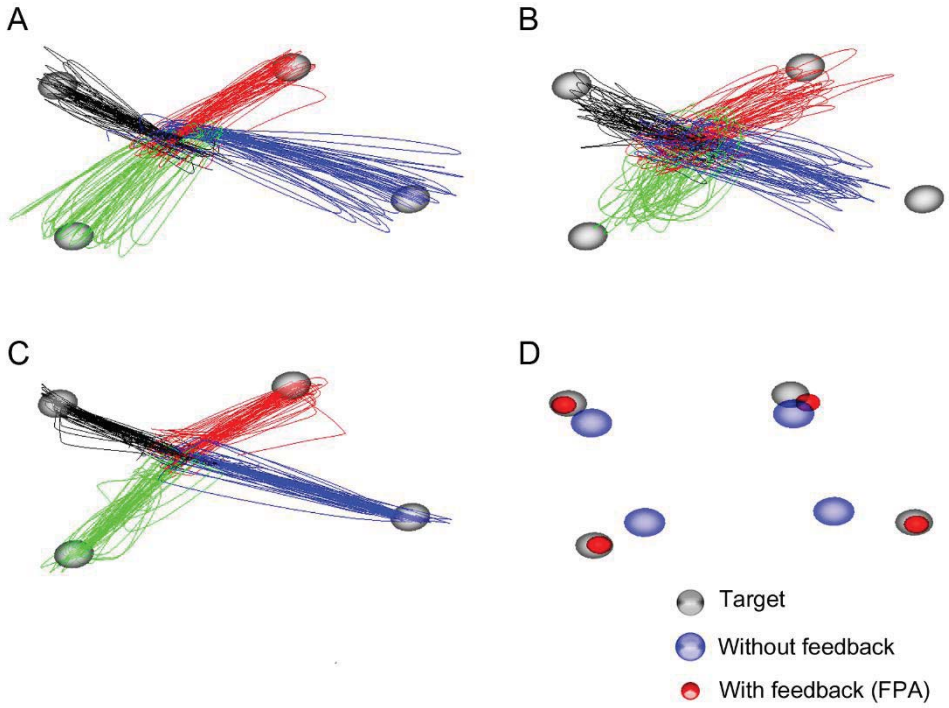

Figure 3-4. Examples of the movement prediction in 3D space in cases with feedback (FPA) and without feedback. The four color lines illustrate the movement trajectory for the different directions. Gray spheres represent objects. (A) Real movement trajectory. (B) Predicted movement trajectory without feedback. (C) Final predicted movement trajectory with feedback (FPA). (D) Endpoint comparison. Blue spheres indicate endpoints of predicted movement trajectory and red spheres depict endpoints of compensated movement trajectory. Radii of blue and red spheres represent SDs of endpoints in cases with feedback and without feedback, respectively.

3.4. Discussion

I proposed a BMI framework combining image processing with a novel prediction method, the FPA that generates feedback information and modifies movement prediction. The FPA predicts a target in every FPA process based on the neural activity, modifies the predicted direction toward the target and modulates the magnitude of the predicted vector to easily reach the target. Because the target is predicted in every FPA process, the subject can change a movement goal at any time. I demonstrated that combining feedback information for movement prediction considerably improves prediction accuracy. The proposed method will improve the performance of the arm-control BMI system not only for non-invasive but also for invasive neural signals. Therefore, the FPA will promote the development of a practical BMI system.

3.4.1. Importance of Feedback Information

Feedback information is very important in movement control. To generate a reaching movement, three processes are required (Kandel, 2012). First, in the movement planning process, the movement needs to be planned to determine the movement direction and distance based on the sensory information about the object and hand locations. Second, in the process of inverse kinematic transformation, the joint angle

trajectories of the shoulder and the elbow are determined to achieve the movement. Third, in the process of inverse dynamic transformation, the torque of the shoulder and elbow should be calculated based on the angle trajectories. The three processes are called sensorimotor transformations and are achieved based on the relationship between the joint angles of the arm and the location of the hand in space.

However, neural representations of the relationship may not exactly describe the real relationships because of structural differences or errors in the model′s parameters (Kandel, 2012). Therefore, this causes movement inaccuracies and it is difficult to predict a movement exactly without feedback information.

To overcome the inaccuracy, I suggested the BMI framework with the FPA. The predicted movements with feedback (FPA) almost did reach the target by modifying the direction and magnitude of the predicted movement vector, although the predicted trajectory without feedback does not reach the target (Fig. 3-4).

A recent study also proposed a BMI that combined target information (Shanechi et al., 2013). The suggested study method predicts the target from neural activity before movement initiation in the first stage and combines the predicted target with the trajectory prediction in the second stage. Although the study is similar to my study in terms of combining position information for movement prediction, there are several limitations. In the previous study, the object positions were determined and fixed on the screen. Therefore, the method cannot be applied to control a neural prosthesis

because the object positions are unknown in real life. This differs to my method, in which BMI obtains the object position from image processing. Moreover, the method predicts the target once before the movement and utilizes it during the trajectory prediction. This causes two main problems. Firstly, if the initial prediction is incorrect, then the target information will disrupt the subsequent prediction. Secondly, although the initial prediction is correct, the user cannot change the movement goal until one trial ends. In contrast, the proposed algorithm, FPA, predicts the target in every time step, therefore several incorrect predictions do not critically affect the trajectory prediction and the user can change the movement goal at any time. Lastly, information about the start and end times of the trials is required to predict the target and trajectory separately, which is inappropriate for practical BMI.

In other BMI studies, the target information was also used to assist the cursor control during the training periods for the adaptation of the subject to the system (Velliste et al., 2008, Fraser et al., 2009) or to determine the parameters of a prediction model (Mulliken et al., 2008). However, the method requires target information. As described above, the method also cannot be used in real life because the target will be changed in various situations.

3.4.2. Feasibility of Practical Brain-Machine Interfaces

The proposed BMI framework with FPA will enable the practical BMI. First, the suggested algorithm improves prediction accuracy, as mentioned above. Second, it is applicable regardless of the object number or position because the FPA uses the positions obtained from the image and the image processing is not affected by the number or position of the object. Third, the subject can change a target at any time because the FPA selects a target based on neural activity and compensates the prediction in every time step (Figs. 3-1 and 3-2). Last, the suggested method can also be applicable to any patients regardless of their disability type because it uses the additional information obtained from an external camera. Moreover, it may be possible to provide automatic grasping control signals using image information regardless of the various sizes and shapes of objects, without decoding the sophisticated finger movement. Therefore, the proposed BMI framework with FPA will promote the realization and commercialization of BMI.

3.4.3. Limitations

The FPA is effective only if the movements are predictable from neural activity. Although the FPA improves prediction accuracy in most cases, it may not improve the performance when the movement prediction is extremely inaccurate because the

algorithm compensates the movement based on the position of the target, which is predicted from neural activity. For this reason, subjects 2 and 9 show relatively little improvement, although the errors were significantly reduced. For the same reason, in case objects are very close to each other, performance improvements by the FPA may be decreased because it is difficult to predict the target from neural activity.

Another limitation is that the proposed method requires an external camera. Therefore, the adherence of a camera may be cumbersome. Nevertheless, it may be more convenient for the user, because it will innovatively improve the performance.

Chapter 4: Transition of Brain Connectivity

4.1. Introduction

In previous chapters, I showed that movement trajectory could be predicted from non-invasive signals and the accuracy could be increased using feedback signals. However, we do not perform continuous movements in daily life. A recent study shows that continuous movement prediction may cause a serious error during a resting state (Velliste et al., 2014). Although the prediction algorithm is optimized for neural signals during movements, it is improper for resting state and causes serious problems. Therefore, the BMI user should be able to turn on or turn off the system or change the system mode. Different brain mechanisms are involved in different brain states that can be measured by functional connectivity. Therefore, the BMI mode will be adjustable using functional connectivity. Moreover, understanding the motor control mechanism of brain will provide important information for movement prediction. Therefore, I aimed to investigate the motor mechanism on reaching movements and transition of functional connectivity according to the movement states.

Studies on the brain mechanism of motor control has been performed from about 150 years before (Schwartz, 2016). There has been controversy on motor control mechanism between feedforward control and feedback control for more than 100 years (Desmurget and Grafton, 2003, Schwartz, 2016). The sensory feedback had

been considered important for motor control for a long time (Mott and Sherrington, 1895, Sherrington, 1910, Lassek and Moyer, 1953, Twitchell, 1954, Lassek, 1955). However the idea was challenged by studies during 1960s and the 1980s (Knapp et al., 1963, Taub and Berman, 1968, Bossom, 1972, 1974, Polit and Bizzi, 1979, Hollerbach, 1982). The studies showed that deafferented animals could recover their motor functions (Knapp et al., 1963, Taub and Berman, 1968, Bossom, 1972, 1974) and they could reach to the targets with sufficient accuracy (Polit and Bizzi, 1979). The results were also confirmed in human (Kelso and Holt, 1980, Rothwell et al., 1982, Sanes et al., 1985). Moreover, Hollerbach argued that transmission delays of sensory feedback, on the order of tens of milliseconds, were too slow to be used as a feedback for stable motor control (Hollerbach, 1982). As a result, the feedforward view was dominant (Rothwell et al., 1982).

Carlton suggested another view on the controversy (Carlton, 1981). He hypothesized that visual feedback would be used not during initial and middle of the movements but during end of the movements. In his study, 0%, 25%, 50%, 75% or 93% of movement trajectories were hidden during reaching. The movement accuracy was not different in the 0% and 50% but different in the 75% and 93%. The view was firmly supported in similar experiments (Zelaznik et al., 1983, Beaubaton and Hay, 1986). Based on these results, it becomes generally accepted that reaching movements are segmented into two states: forward control before sensory feedback and feedback control (Desmurget and Grafton, 2003, Friston, 2011).

In 2002, optimal feedback control (OFC) using efference copy signals was proposed (Todorov and Jordan, 2002). The model compensates movement errors using the efference copy of motor commands before sensory feedback (Scott, 2004). The suggestion of the OFC increases the importance of the sensory feedback in the motor control again. The OFC theory has been commonly accepted as a motor control mechanism (Scott, 2004, Hudson et al., 2010, Scott, 2012, Schwartz, 2016). The OFC model was suggested and used in the context of that the characteristics of behavior is similar with the optimal control theory (Todorov and Jordan, 2002, Scott, 2004, 2012). However, there are studies that humans do not behave optimally (Hudson et al., 2010, Kistemaker et al., 2010, de Rugy et al., 2012) and other models have also been suggested (Feldman and Levin, 2009, Friston, 2011, Loeb, 2012).

In the OFC model, the brain compensates the motor command using efference copy before sensory feedback. However, it is inefficient that the brain change the decision without any new information. If the brain is an efficient system, the brain should decide motor commands based on all knowledge already known. Therefore, all motor related areas should share their information before the movements and then the motor command should be compensated by sensory feedback during movements.

To verify the motor control mechanism, it is essential to examine the neurophysiology of the brain during movements. Many brain areas are involved in motor control with interaction among these areas (Scott, 2004, 2012). Moreover, the roles of the brain areas are changed according to the time flow. Therefore, interaction among motor

related areas of whole brain should be examined according to time. Although there are studies measuring connectivity of several brain areas at movement duration (Chen et al., 2010, van Wijk et al., 2013, Boenstrup et al., 2014, Pool et al., 2014, Volz et al., 2015, Bonstrup et al., 2016), to the best of my knowledge, there is no electrophysiology study on how brain mechanism is translated according to the time flow.

Here I measured whole brain MEG signals of human during goal-directed reaching movements. Source activities of 24 motor related areas were extracted using a Beamforming method. Functional connectivity was calculated with mutual information (MI) among source areas according to the time flow. Degree centrality was calculated at each time.

4.2. Methods

4.2.1. Experimental Procedure and Data Acquisition

To investigate motor mechanism, previous MEG data during reaching describe in Chapter 2 was analyzed.

4.2.2. Source Signal Extraction

To examine the activities of the motor related area, source activities were calculated from 24 region of interest (ROI). The 24 ROI were left and right of prefrontal area (PF), SMA, dorsal premotor (PMd), M1, S1, anterior cingulate cortex (ACC), putamen (PUT), pallidum (PAL), thalamus (THA), PPC, V1 and CB, respectively. The MEG and MRI data were aligned according to the three anatomical landmarks (i.e., nasion, left and right preauricular). The 24 ROI positions were calculated by averaging relevant AAL atlas positions.

I created a lead field matrix, which describes the relation between MEG signals and source activities, on the points with a spherical head model (Cuffin and Cohen, 1979). If I define B as MEG signals, the relation could be described as follows;

$$B = A \cdot S + n$$

where S represents source activities, n denotes the measurement noise, and A is a lead field matrix.

Because the signal at each point consisted of two orthogonal dipole components tangential to the surface of a spherical head model, the source model consisted of two source vectors for each point. To calculate the source model, standardized low resolution brain electromagnetic tomography (sLORETA) algorithm was used (Pascual-Marqui, 2002).

The current density at the j-th point, S_j, is given by

$$S_j = W_j \cdot B$$

To combine the two source vectors, a principal component of the sources was calculated by singular value decomposition (SVD).

4.2.3. Functional Connectivity

To investigate the motor mechanism, I calculated functional connectivity according to the time flow. The source activities were band-pass filtered to low (0.5 - 8 Hz), alpha (8 -13 Hz), beta (13 − 30 Hz) and gamma (30 - 200 Hz) frequency bands. The filtered signals of 24 ROIs were temporally segmented based on a movement onset. Movement response time to the visual stimuli was 287.0 ± 201.7 ms (mean ± SD).

Because large variation of the response time could change the brain activity pattern, the trials were selected that the response time was within 100 - 400 ms (72.28 % of whole trials) for further analysis. To obtain functional connectivity, mutual information (MI) between source activities was computed with 10ms interval from -500ms to 500ms based on movement onset. Window size for MI calculation was 100ms. Ninety milliseconds of the window were overlapped. The MI was calculated with the following equation:

$$\mathrm{MI}(x_1, x_2) = \sum_{x_1, x_2} p(x_1, x_2) \log \frac{p(x_1, x_2)}{p(x_1)p(x_2)}$$

where x_1 and x_2 are the source signals of the 24 ROIs; $p(x_1)$ and $p(x_2)$ indicate probability density function (PDF) of x_1 and x_2, respectively; $p(x_1, x_2)$ denotes the joint PDF of x_1 and x_2. The PDFs were calculated from 100ms window data of all trials at each time. The MI matrices were averaged by subjects for each frequency band.

To find importance ROIs in the motor network, *degree* centralities were calculated which is equal to the summation of links connected to that node. Therefore it reflects importance of the node in the network (Rubinov and Sporns, 2010). The degree is one of the most common measures of centrality (Rubinov and Sporns, 2010). Centrality is an effective method to represent the summary of the connectivity (Burns et al., 2014). To highlight the transition of the motor network, baseline correction was performed by subtracting the mean centrality during baseline. The duration of the baseline was

from -500ms to -400ms. Therefore a positive value implies that the centrality is increased during movements than resting state (baseline). A negative value means the opposite.

4.2.4. K-Means Clustering

To uncover a finite set of the motor network, I used unsupervised clustering algorithm, K-means, for each frequency band (Burns et al., 2014). The K-means algorithm separates the motor networks into K states. In my study, I sorted the networks into 10 states which are large enough to reduce a loss of possible motor networks. The centralities over time were clustered by using the K-means algorithm with nonrandom centroid seeds. To determine the centroid seeds, I separated same 10 intervals and averaged the centralities within each interval. The 10 averaged centralities were used as the centroid seeds. After the clustering, centralities of same cluster were averaged. As a result, 10 motor networks were determined for each frequency band.

4.2.5. Visualization of the Connectivity

For intuitive presentation, I illustrated the connectivity and centrality on the brain model. The connectivity (MI) was represented as a thickness of an edge between ROIs. The centrality determined a size of a node. Only the connectivity and the centrality were described which is larger than baseline. Therefore the thickness of the edge and the node size show that how much the connectivity and centrality are increased according to the movement planning and execution. The maximum sizes of edge and node were limited. To visualize the connectivity on brain model, I used BrainNet Viewer (Xia et al., 2013). The data analysis procedure is summarized in Fig. 4-1.

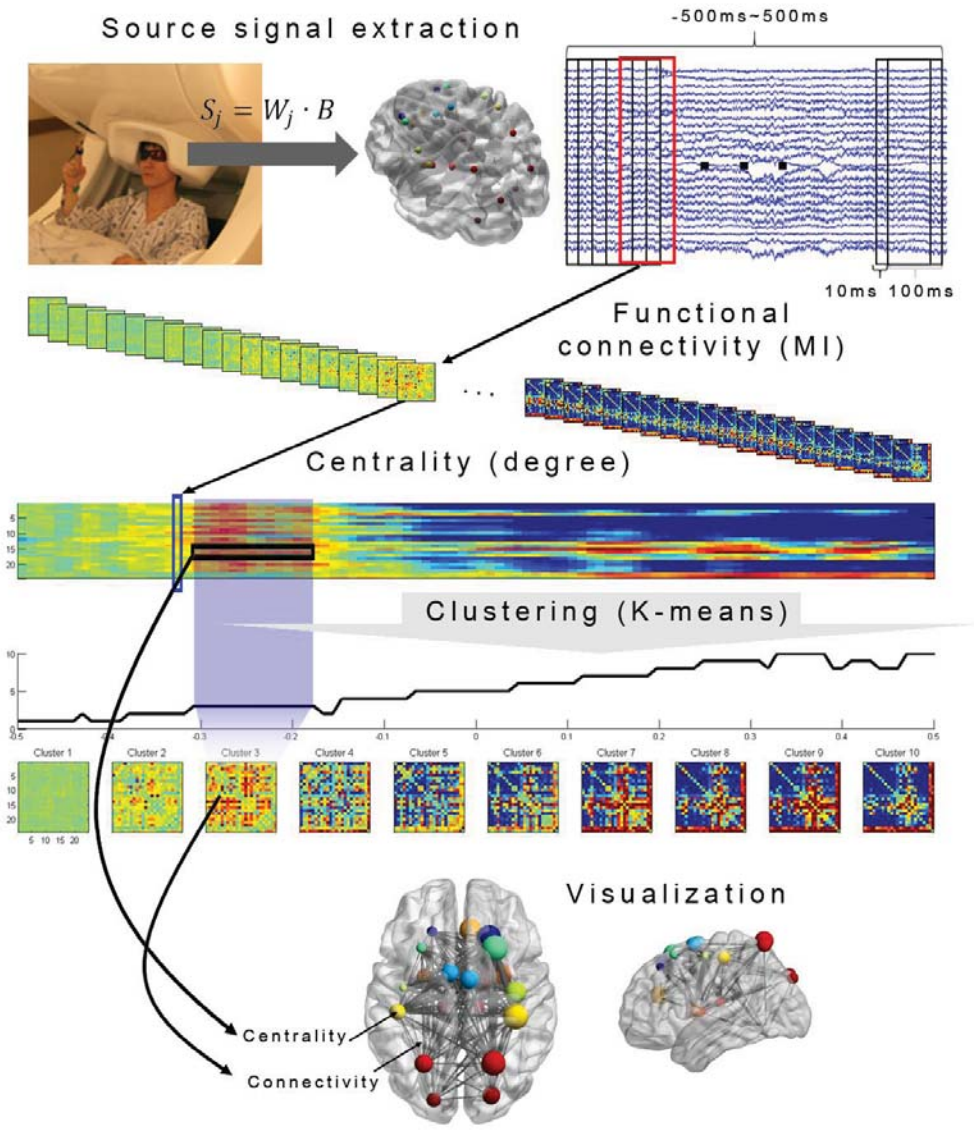

Figure 4-1. Schematic diagram of data analysis procedures. To examine the activities of the motor related area, source activities were calculated from 24 region of interest (ROI). After the band-pass filter and signal segmentation, mutual information (MI) between source activities was computed with 10ms interval from -500ms to 500ms. Window size for MI calculation was 100ms. To find importance ROIs in the motor

network, degree centralities were calculated. To uncover a finite set of the motor network, I used unsupervised clustering algorithm, K-means, for each frequency band. For intuitive presentation, I illustrated the connectivity on the brain model using BrainNet Viewer. The connectivity (MI) was represented as a thickness of an edge between ROIs. The centrality determined a size of a node.

4.3. Results

Most of the centralities were decreased in alpha, beta and gamma bands before and during movements (Fig. 4-2). Whereas some centralities in low-frequency were increased. Because only the centralities of low-frequency were increased, activity of low-frequency was mainly presented to reveal the important area according to the movements (Fig. 4-3). Centralities of different frequency bands were shown according to time in Fig. 4-2. Each line represents the centrality of one ROI. The centralities were normalized by mean and standard deviation (SD) of baseline (from -500ms to -400ms). Transparent red thick line shows 3 SD.

The centralities of most of the motor related area were increased before movements in low-frequency (Fig. 4-3). Whereas, the centralities of several area such as CB and basal ganglia (PUT and PAL) were increased during reaching movements in low-frequency. In the figure, red color represents the increase of centralities, whereas blue means decreased centralities (Fig. 4-3A). The x-axis denotes time and the y-axis depicts 24 ROIs. Clusters of the centralities in low-frequency were illustrated in Fig. 4-3(B). Fig. 4-3(C) shows the arm position. Corresponding connectivities of each cluster were represented in Fig. 4-3(D). For intuitive presentation, the centralities and connectivities were depicted on the brain model in Fig. 4-3(E).

Ten clusters can be explained in several brain states (Fig. 4-4). We assigned the several clusters into one state based on the similarity and behavioral data (Fig. 4-3(C)). Cluster 1 was resting state before target presentation. Cluster 2 may be motor planning after the target presentation. Cluster 3-6 may be related to generation of the motor command and sending it to the peripheral. In the motor command state, centralities of SMA and BG were high. Cluster 7-8 during movements can be interpreted as motor execution state. In the execution state, CB was included and SMA was excluded as

important players. Cluster 9-10 corresponded to the brain state after movement. We called it as ″recovery″ state. Brain networks of cluster 3, 7, and 9 were illustrated in Fig 4-4 to represent the motor command, execution, and recovery state, respectively. Fig. 4-5 depicts the increase and decrease of centralities on 24 ROIs before (from -400ms to -200ms) and during (from 0ms to 500ms) movements compared to the baseline (from -500ms to -400ms). Statistical significance was evaluated by paired sample t-test. Black bars illustrate the centralities before movements, whereas gray bars depict the centralities during movements. The error bars show the standard error of mean (SEM). Stars on the bars denote significance levels. Statistical significances were calculated between increased centralities and baseline centralities for each ROI. Most of centralities were increased before movements except the left CB (ROI 23). Whereas centralities only on several area, left PUT (ROI 13), left and right PAL (ROI 15 and 16), left and right CB (ROI 23 and 24), were increased during movements.

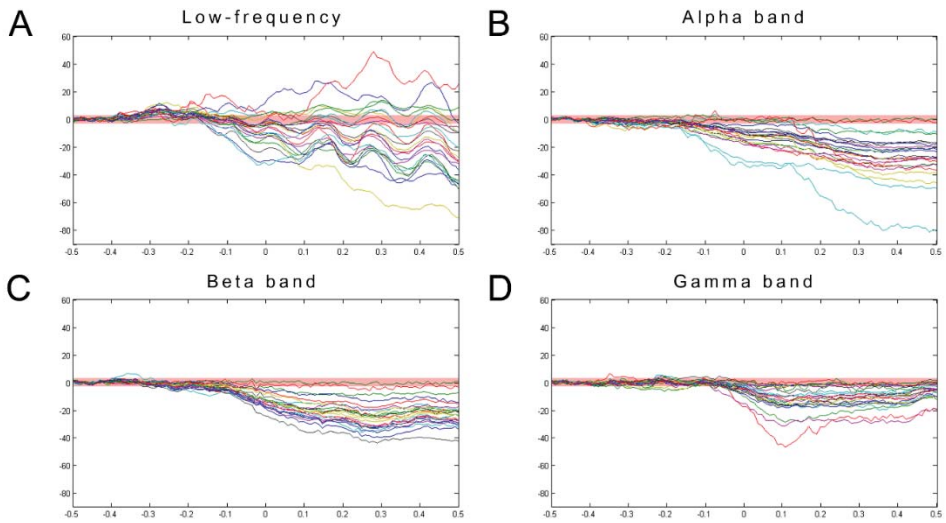

Figure 4-2. Centralities of 24 ROIs in each frequency band. (A) Centralities of low-frequency, (B) alpha band, (C) beta band, (D) gamma band, respectively. Each line

represents the centrality of one ROI. The centralities were normalized by mean and standard deviation (SD) of baseline (-500ms to -400ms). Transparent red thick line shows 3 SD.

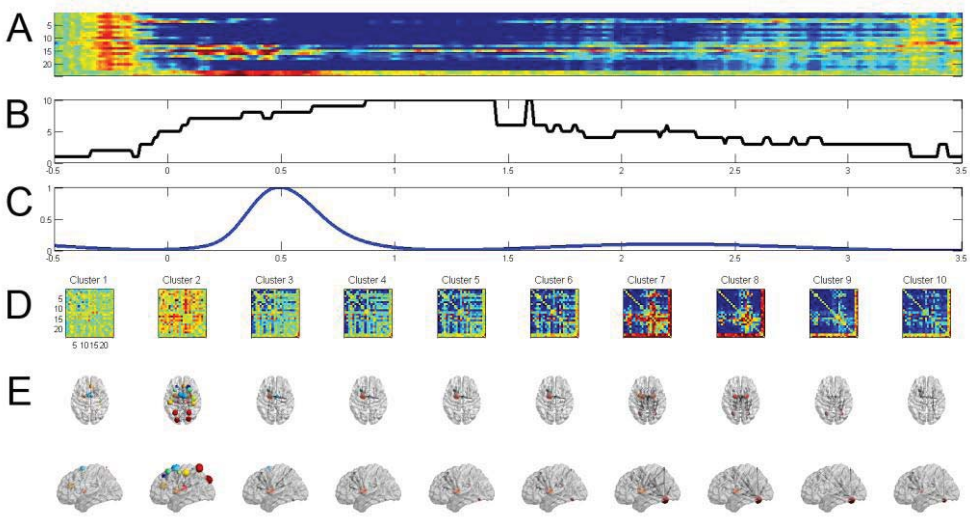

Figure 4-3. Transition of centralities and connectivities before and during reaching movements. (A) Transition of the centralities of low-frequency band. Red color represents the increase of centralities, whereas blue means decreased centralities. The x-axis denotes time and the y-axis depicts 24 ROIs. (B) Clusters of the centralities in low-frequency. (C) Arm position. (D) Corresponding connectivities of each cluster. (E) The centralities and connectivities on the brain model.

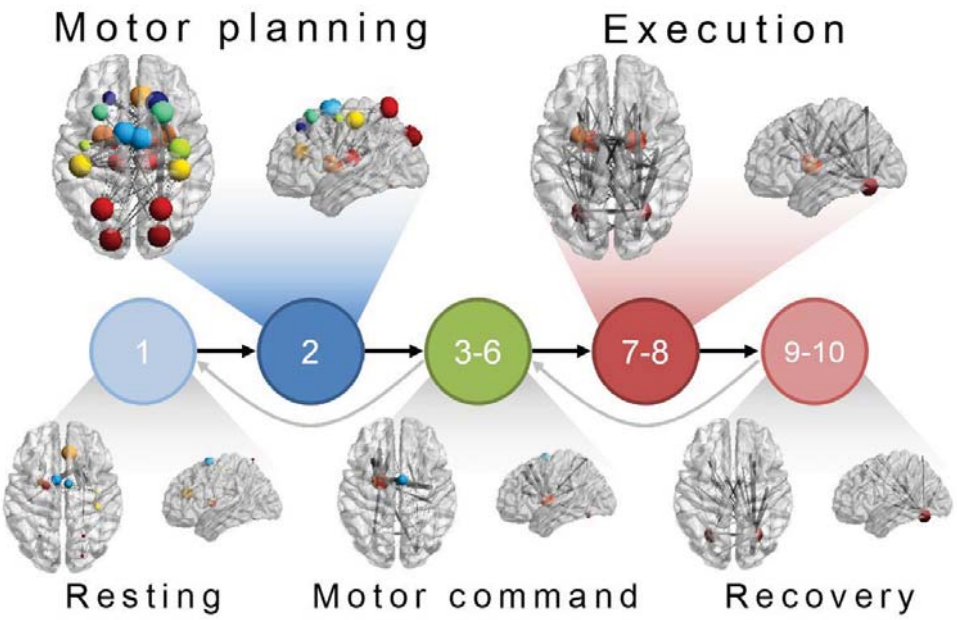

Figure 4-4 State transition diagrams. It shows the state transition corresponding to Fig. 4-3(B). Different brain states have different networks. We assigned the several clusters into one state based on the similarity and behavioral data (Fig. 4-3(C)). Black arrows denote the state flow from resting to motor execution. Sky blue arrows represent the state change after the movements. Motor command state means generation and sending of the motor command.

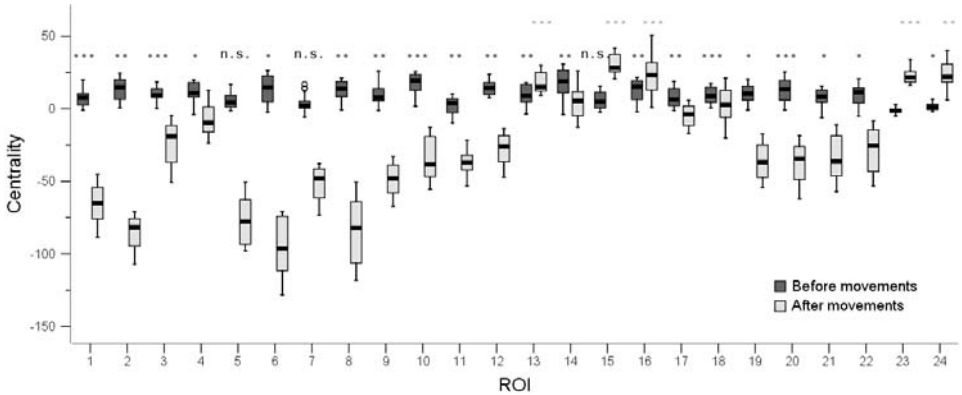

Figure 4-5. The increase and decrease of centralities on 24 ROIs before (from -400ms to -200ms) and during (from 0ms to 500ms) movements compared to the baseline (from -500ms to -400ms). Black bars illustrate the centralities before movements, whereas gray bars depict the centralities during movements. The error bars show the standard error of mean (SEM). Stars on the bars denote significance levels (*$p < 0.05$, **$p < 0.01$, ***$p < 0.001$ by paired-sample t-test). Statistical significances were calculated between increased centralities and baseline centralities for each ROI. ROI 1: left PF, 2: right PF, 3: left SMA, 4: right SMA, 5: left PMd, 6: right PMd, 7: left M1, 8: right M1, 9: left S1, 10: right S1, 11: left ACC, 12: right ACC, 13: left PUT, 14: right PUT, 15: left PAL, 16: right PAL, 17: left THA, 18: right THA, 19: left PPC, 20: right PPC, 21: left V1, 22: right V1, 23: left CB and 24: right CB.

4.4. Discussion

The motor control mechanism has long been studied. However, it is still debating. I hypothesized that all motor related areas will be involved before movements and it will be modulated by sensory feedback. In this study, I investigated the transition of brain connectivity among motor related areas in different frequency bands. The results demonstrated that motor mechanisms were different before (feedforward control) and during movements (feedback control). Moreover, I showed that the simpler control mechanism is applied during movements. It may be beneficial for fast motor response. The results also revealed that oscillations in low-frequency play an important role in motor control. The results may provide useful information to develop BMI systems.

4.4.1. Different Mechanism for Feedforward Feedback Control

There has been controversy on motor control mechanism between feedforward control and feedback control for a long time. Although it is now commonly accepted that movements are controlled by feedforward control before sensory feedback and by feedback control during movements with the feedback, to my best knowledge, the change of the motor control mechanism was not neurophysiologically examined. The results showed that the motor networks change according to before movement (feedforward control) and during the movement (feedback control). Although there have been studies that show the neural activities before and during the movements, it

is the first time that reveals a transition of the interactions among multiple motor related area according to the time. Therefore the results directly demonstrate the theory that different mechanisms are involved in motor control.

However, there is an import difference between previous theory and the result. Up to now, it has been generally assumed that the feedback controller consists of feedforward controller and present state estimator with sensory feedback to compensate the feedforward controller (Scott, 2004, 2012, Kandel et al., 2013). Therefore, it has been considered that more brain areas will be involved in feedback motor control. However, the results show that lots of interaction among motor related areas were reduced during reaching movements. Only interactions with CB and BG (PUT and PAL) were increased. The results imply that feedback control mechanism is simpler than feedforward mechanism. The simple mechanism during movements may explain fast movement response. It seems that important decisions for motor control such as movement direction, distance and speed is determined before movements and simple correction to achieve the goal is performed during movements. Therefore neural activities during motor planning could contain substantial information for motor control. The planning period may be useful for the BMI

4.4.2. Importance of Low-Frequency in Motor Control

Most of interactions in alpha, beta and gamma band were decreased during movements, whereas interactions of several areas in low-frequency were quite increased. Moreover, interactions among most of motor related areas in low-frequency were increased before movements that may related to the motor planning. The results imply that low-frequency are especially important not only for motor planning but also for motor execution. It may be related to that neural oscillations of low-frequency contains substantial movement information such as movement trajectories or velocities (Zelaznik et al., 1983, Schalk et al., 2007, Pistohl et al., 2008, Waldert et al., 2008, Waldert et al., 2009, Yeom et al., 2013). Moreover the results suggest that information of movements are not only processed but also transmitted in low-frequency oscillation. It may provide useful information to BMI system to estimate the user state using low-frequency connectivities.

4.4.5. Limitations

The results not mean that other motor related areas are not involved during movements except CB and basal ganglia. Although the CB and basal ganglia play as a hub, other areas are still working. Examining the centralities are a good method to find important areas in the motor networks, it is difficult to reveal a causal relationship among these areas. To model the motor control mechanism, further studies are required.

Chapter 5: Conclusion

Previous BMI studies selecting options were restrictive. In this thesis, I showed that the movement trajectories can be predicted from non-invasive MEG signals. It implies that unlimited movement may be possible by controlling the robotic arm based on prediction. Moreover, the performance of movement prediction can be highly increased using feedback information. To use the BMI system in real life, the BMI users should also be able to turn on or turn off the system or change the system mode, because we do not perform continuous movements in daily life. I also showed that the functional connectivity is changed according to the brain states. Using the property, selecting the BMI mode or switching the system will be possible.

Based on my study results, I suggest the direction of future BMI system for the practical use. In real life, we encounter various situations. In the situation, we do lots of things such as eating food, communicating with others, and moving to destination. Therefore, the BMI system should predict the brain states and change the BMI mode continuously. Because different brain state has a different probabilistic density function (PDF) of the brain connectivity, we can estimate the brain state using the connectivity (Fig. 5-1). The PDFs of the brain states can be calculated from each subject or database of many subjects. For the system stability, other context can be additionally used to restrict the change of the BMI mode such as individual personality,

life style, time or surroundings. The brain state can be predicted using an algorithm such as maximum likelihood estimation (MLE).

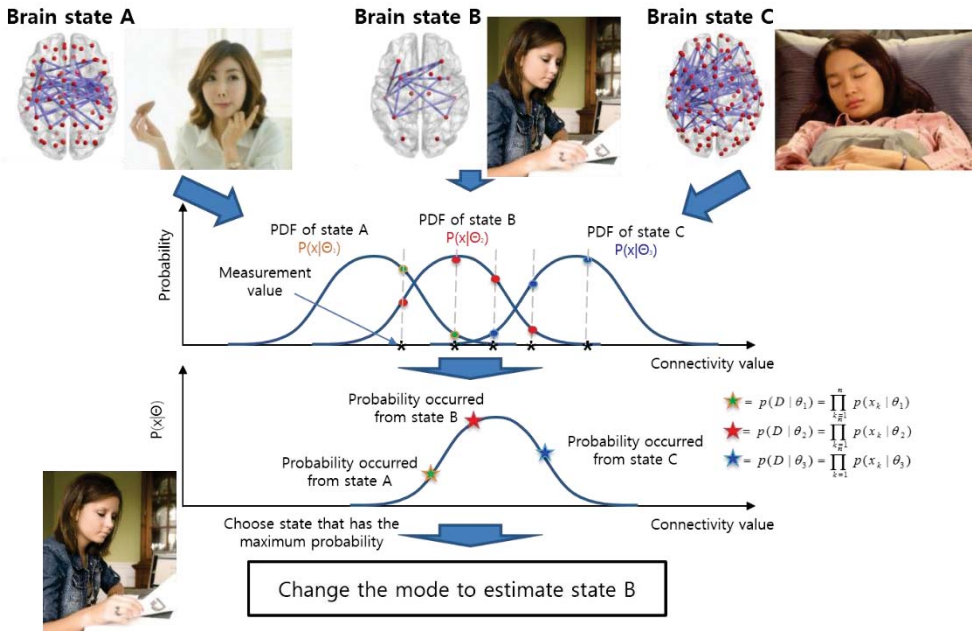

Figure 5-1. Prediction of the brain state. The brain states can be predicted using the brain connectivity based on probabilistic algorithm such as maximum likelihood estimation (MLE).

In case of that the BMI mode is the movement control, the system will predict the movement parameters from motor planning such as a movement direction, distance or maximum speed because most of important processes for motor control may be finished before the movement (Fig. 5-2). Then the movement prediction should be

compensated by feedback signals during movements. Combining brain states and feedback information may make practical BMI possible.

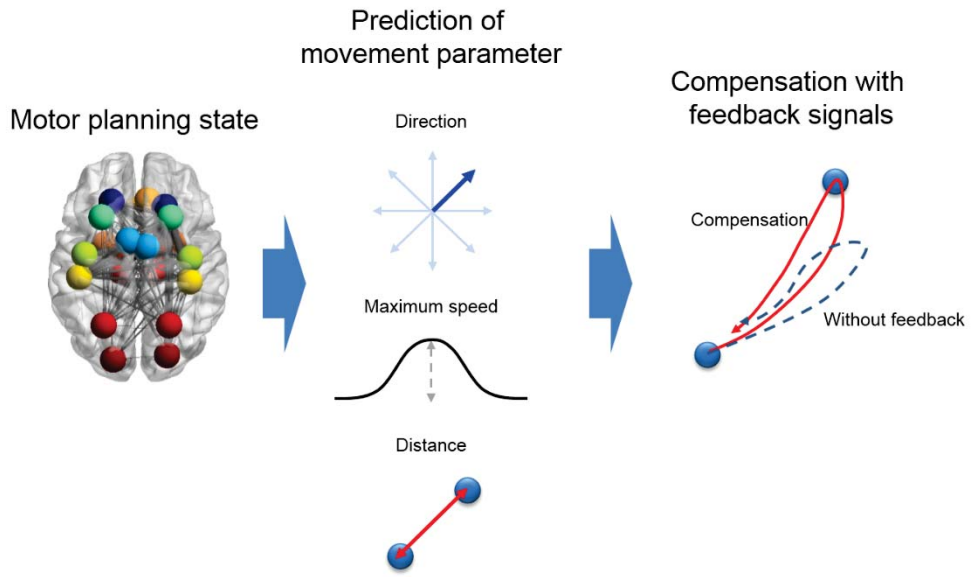

Figure 5-2. Movement control mode. The system predicts the movement parameters from motor planning such as a movement direction, distance, or maximum speed. Then the movement prediction should be compensated by feedback signals during movements.

REFERENCES

Beaubaton D, Hay L (1986) Contribution of visual information to feedforward and feedback processes in rapid pointing movements. Human Movement Science 5:19-34.

Boenstrup M, Feldheim J, Heise K, Gerloff C, Hummel FC (2014) The control of complex finger movements by directional information flow between mesial frontocentral areas and the primary motor cortex. The European journal of neuroscience 40:2888-2897.

Bonstrup M, Schulz R, Feldheim J, Hummel FC, Gerloff C (2016) Dynamic causal modelling of EEG and fMRI to characterize network architectures in a simple motor task. NeuroImage 124:498-508.

Bossom J (1972) Time of recovery of voluntary movement following dorsal rhizotomy. Brain research 45:247-250.

Bossom J (1974) Movement without proprioception. Brain research 71:285-296.

Bradberry TJ, Gentili RJ, Contreras-Vidal JL (2010) Reconstructing Three-Dimensional Hand Movements from Noninvasive Electroencephalographic Signals. J Neurosci 30:3432-3437.

Bradberry TJ, Rong F, Contreras-Vidal JL (2009) Decoding center-out hand velocity from MEG signals during visuomotor adaptation. Neuroimage 47:1691-1700.

Burns SP, Santaniello S, Yaffe RB, Jouny CC, Crone NE, Bergey GK, Anderson WS, Sarma SV (2014) Network dynamics of the brain and influence of the epileptic seizure onset zone. Proceedings of the National Academy of Sciences of the United States of America 111:E5321-5330.

Carlton LG (1981) Processing visual feedback information for movement control. Journal of experimental psychology Human perception and performance 7:1019-1030.

Chen CC, Kilner JM, Friston KJ, Kiebel SJ, Jolly RK, Ward NS (2010) Nonlinear coupling in the human motor system. The Journal of neuroscience : the

official journal of the Society for Neuroscience 30:8393-8399.

Collinger JL, Wodlinger B, Downey JE, Wang W, Tyler-Kabara EC, Weber DJ, McMorland AJ, Velliste M, Boninger ML, Schwartz AB (2013) High-performance neuroprosthetic control by an individual with tetraplegia. Lancet 381:557-564.

Cuffin BN, Cohen D (1979) Comparison of the magnetoencephalogram and electroencephalogram. Electroencephalography and clinical neurophysiology 47:132-146.

de Rugy A, Loeb GE, Carroll TJ (2012) Muscle coordination is habitual rather than optimal. The Journal of neuroscience : the official journal of the Society for Neuroscience 32:7384-7391.

Desmurget M, Grafton S (2003) Feedback or Feedforward Control: End of a Dichotomy. Taking action: Cognitive neuroscience perspectives on intentional acts 289.

Dornhege G (2007) Toward brain-computer interfacing. Cambridge, Mass. ; London: MIT.

Duda RO, Hart PE, Stork DG (2001) Pattern classification. New York ; Chichester: Wiley.

Feldman AG, Levin MF (2009) The equilibrium-point hypothesis--past, present and future. Advances in experimental medicine and biology 629:699-726.

Flint RD, Lindberg EW, Jordan LR, Miller LE, Slutzky MW (2012) Accurate decoding of reaching movements from field potentials in the absence of spikes. J Neural Eng 9.

Fraser GW, Chase SM, Whitford A, Schwartz AB (2009) Control of a brain-computer interface without spike sorting. J Neural Eng 6.

Friston K (2011) What is optimal about motor control? Neuron 72:488-498.

Ganguly K, Secundo L, Ranade G, Orsborn A, Chang EF, Dimitrov DF, Wallis JD, Barbaro NM, Knight RT, Carmena JM (2009) Cortical Representation of Ipsilateral Arm Movements in Monkey and Man. J Neurosci 29:12948-12956.

Georgopoulos AP, Kalaska JF, Caminiti R, Massey JT (1982) On the relations between the direction of two-dimensional arm movements and cell

discharge in primate motor cortex. The Journal of neuroscience : the official journal of the Society for Neuroscience 2:1527-1537.

Georgopoulos AP, Schwartz AB, Kettner RE (1986) Neuronal population coding of movement direction. Science 233:1416-1419.

Haralick RM, Shapiro LG (1985) Image Segmentation Techniques. Comput Vision Graph 29:100-132.

Hauschild M, Mulliken GH, Fineman I, Loeb GE, Andersen RA (2012) Cognitive signals for brain-machine interfaces in posterior parietal cortex include continuous 3D trajectory commands. Proceedings of the National Academy of Sciences of the United States of America 109:17075-17080.

Hochberg LR, Bacher D, Jarosiewicz B, Masse NY, Simeral JD, Vogel J, Haddadin S, Liu J, Cash SS, van der Smagt P, Donoghue JP (2012) Reach and grasp by people with tetraplegia using a neurally controlled robotic arm. Nature 485:372-375.

Hollerbach JM (1982) Computers, brains, and the control of movement. Cambridge, Mass.: Massachusetts Institute of Technology, Artificial Intelligence Laboratory.

Hudson TE, Tassinari H, Landy MS (2010) Compensation for changing motor uncertainty. PLoS computational biology 6:e1000982.

Ince NF, Gupta R, Arica S, Tewfik AH, Ashe J, Pellizzer G (2010) High accuracy decoding of movement target direction in non-human primates based on common spatial patterns of local field potentials. PloS one 5:e14384.

Judy JW (2012) Neural Interfaces for Upper-Limb Prosthesis Control. Ieee Pulse 3:57-60.

Kandel ER (2012) Principles of neural science. New York: McGraw-Hill.

Kandel ER, Schwartz JH, Jessell TM, Siegelbaum S, Hudspeth AJ (2013) Principles of neural science. New York, NY ; London: McGraw-Hill.

Kelso JA, Holt KG (1980) Exploring a vibratory systems analysis of human movement production. Journal of neurophysiology 43:1183-1196.

Kennison SM Introduction to Language Development.

Kim SP, Simeral JD, Hochberg LR, Donoghue JP, Black MJ (2008) Neural control of computer cursor velocity by decoding motor cortical spiking activity in

humans with tetraplegia. Journal of neural engineering 5:455-476.

Kim SP, Simeral JD, Hochberg LR, Donoghue JP, Friehs GM, Black MJ (2011) Point-and-click cursor control with an intracortical neural interface system by humans with tetraplegia. IEEE transactions on neural systems and rehabilitation engineering : a publication of the IEEE Engineering in Medicine and Biology Society 19:193-203.

Kistemaker DA, Wong JD, Gribble PL (2010) The central nervous system does not minimize energy cost in arm movements. Journal of neurophysiology 104:2985-2994.

Knapp HD, Taub E, Berman AJ (1963) Movements in monkeys with deafferented forelimbs. Experimental neurology 7:305-315.

Lassek AM (1955) Effect of combined afferent lesions on motor function. Neurology 5:269-272.

Lassek AM, Moyer EK (1953) An ontogenetic study of motor deficits following dorsal brachial rhizotomy. Journal of neurophysiology 16:247-251.

Lebedev MA, Nicolelis MA (2006) Brain-machine interfaces: past, present and future. Trends in neurosciences 29:536-546.

Loeb GE (2012) Optimal isn't good enough. Biological cybernetics 106:757-765.

MacKenzie IS, Kauppinen T, Silfverberg M (2001) Accuracy measures for evaluating computer pointing devices. In: Proceedings of the SIGCHI Conference on Human Factors in Computing Systems, pp 9-16 Seattle, Washington, USA: ACM.

Mott FW, Sherrington CS (1895) Experiments upon the influence of sensory nerves upon movement and nutrition of the limbs : preliminary communication. London: Harrison & Sons, printers ...

Mulliken GH, Musallam S, Andersen RA (2008) Decoding trajectories from posterior parietal cortex ensembles. J Neurosci 28:12913-12926.

Murphy KP (2012) Machine learning : a probabilistic perspective. Cambridge, Mass. ; London: MIT Press.

Pascual-Marqui RD (2002) Standardized low-resolution brain electromagnetic tomography (sLORETA): technical details. Methods and findings in experimental and clinical pharmacology 24 Suppl D:5-12.

Pistohl T, Ball T, Schulze-Bonhage A, Aertsen A, Mehring C (2008) Prediction of arm movement trajectories from ECoG-recordings in humans. Journal of neuroscience methods 167:105-114.

Polit A, Bizzi E (1979) Characteristics of motor programs underlying arm movements in monkeys. Journal of neurophysiology 42:183-194.

Pool EM, Rehme AK, Fink GR, Eickhoff SB, Grefkes C (2014) Handedness and effective connectivity of the motor system. NeuroImage 99:451-460.

Purves D (2008) Neuroscience. Sunderland, Mass.: Sinauer.

Rickert J, Oliveira SC, Vaadia E, Aertsen A, Rotter S, Mehring C (2005) Encoding of movement direction in different frequency ranges of motor cortical local field potentials. The Journal of neuroscience : the official journal of the Society for Neuroscience 25:8815-8824.

Rothwell JC, Traub MM, Day BL, Obeso JA, Thomas PK, Marsden CD (1982) Manual motor performance in a deafferented man. Brain : a journal of neurology 105 (Pt 3):515-542.

Rubinov M, Sporns O (2010) Complex network measures of brain connectivity: uses and interpretations. NeuroImage 52:1059-1069.

Sanes JN, Mauritz KH, Dalakas MC, Evarts EV (1985) Motor control in humans with large-fiber sensory neuropathy. Human neurobiology 4:101-114.

Santhanam G, Ryu SI, Yu BM, Afshar A, Shenoy KV (2006) A high-performance brain-computer interface. Nature 442:195-198.

Schalk G, Kubanek J, Miller KJ, Anderson NR, Leuthardt EC, Ojemann JG, Limbrick D, Moran D, Gerhardt LA, Wolpaw JR (2007) Decoding two-dimensional movement trajectories using electrocorticographic signals in humans. Journal of neural engineering 4:264-275.

Schwartz AB (2016) Movement: How the Brain Communicates with the World. Cell 164:1122-1135.

Scott SH (2004) Optimal feedback control and the neural basis of volitional motor control. Nature reviews Neuroscience 5:532-546.

Scott SH (2012) The computational and neural basis of voluntary motor control and planning. Trends in cognitive sciences 16:541-549.

Shanechi MM, Williams ZM, Wornell GW, Hu RC, Powers M, Brown EN (2013) A

Real-Time Brain-Machine Interface Combining Motor Target and Trajectory Intent Using an Optimal Feedback Control Design. PloS one 8.

Sherrington CS (1910) Flexion-reflex of the limb, crossed extension-reflex, and reflex stepping and standing. The Journal of physiology 40:28-121.

Taub E, Berman A (1968) Movement and learning in the absence of sensory feedback. The neuropsychology of spatially oriented behavior 173-192.

Taylor DM, Tillery SI, Schwartz AB (2002) Direct cortical control of 3D neuroprosthetic devices. Science 296:1829-1832.

Thrun S, Burgard W, Fox D (2005) Probabilistic robotics. Cambridge, Mass.: MIT Press.

Todorov E, Jordan MI (2002) Optimal feedback control as a theory of motor coordination. Nature neuroscience 5:1226-1235.

Twitchell TE (1954) Sensory factors in purposive movement. Journal of neurophysiology 17:239-252.

van Wijk BC, Litvak V, Friston KJ, Daffertshofer A (2013) Nonlinear coupling between occipital and motor cortex during motor imagery: a dynamic causal modeling study. NeuroImage 71:104-113.

Velliste M, Kennedy SD, Schwartz AB, Whitford AS, Sohn JW, McMorland AJ (2014) Motor cortical correlates of arm resting in the context of a reaching task and implications for prosthetic control. The Journal of neuroscience : the official journal of the Society for Neuroscience 34:6011-6022.

Velliste M, Perel S, Spalding MC, Whitford AS, Schwartz AB (2008) Cortical control of a prosthetic arm for self-feeding. Nature 453:1098-1101.

Volz LJ, Eickhoff SB, Pool EM, Fink GR, Grefkes C (2015) Differential modulation of motor network connectivity during movements of the upper and lower limbs. NeuroImage 119:44-53.

Waldert S, Pistohl T, Braun C, Ball T, Aertsen A, Mehring C (2009) A review on directional information in neural signals for brain-machine interfaces. Journal of physiology, Paris 103:244-254.

Waldert S, Preissl H, Demandt E, Braun C, Birbaumer N, Aertsen A, Mehring C (2008) Hand movement direction decoded from MEG and EEG. The Journal of neuroscience : the official journal of the Society for Neuroscience 28:1000-

1008.

Wessberg J, Stambaugh CR, Kralik JD, Beck PD, Laubach M, Chapin JK, Kim J, Biggs SJ, Srinivasan MA, Nicolelis MA (2000) Real-time prediction of hand trajectory by ensembles of cortical neurons in primates. Nature 408:361-365.

Wolpaw JR, Wolpaw EW (2012) Brain-computer interfaces : principles and practice. New York: Oxford University Press.

Wu W, Black MJ, Mumford D, Gao Y, Bienenstock E, Donoghue JP (2004) Modeling and decoding motor cortical activity using a switching Kalman filter. Ieee T Bio-Med Eng 51:933-942.

Xia M, Wang J, He Y (2013) BrainNet Viewer: a network visualization tool for human brain connectomics. PloS one 8:e68910.

Yeom HG, Kim JS, Chung CK (2013) Estimation of the velocity and trajectory of three-dimensional reaching movements from non-invasive magnetoencephalography signals. Journal of neural engineering 10:026006.

Yeom HG, Kim JS, Chung CK (2014) High-accuracy brain-machine interfaces using feedback information. PloS one 9:e103539.

Zelaznik HZ, Hawkins B, Kisselburgh L (1983) Rapid visual feedback processing in single-aiming movements. Journal of motor behavior 15:217-236.

국문초록

배경: 뇌-기계 인터페이스(BMI)는 몸이 불편한 장애인도 다른 사람과 소통하고 전자장비를 제어하도록 돕는 매우 유용한 기술이다. 최근 침습적인 BMI 연구에서 사지마비 환자가 자신의 뇌파를 이용하여 로봇 팔을 제어해서 사물을 잡는 것을 수행하는 좋은 결과를 보여주었다. 장애인이 로봇 팔을 자신의 팔처럼 제어할 수 있다면 많은 것을 할 수 있기 때문에 이 연구결과는 매우 의미가 있다. 하지만 침습적 방법은 뇌세포의 손상을 야기할 수 있으며, 장기간 측정 시 불안정하다는 단점이 있다. 따라서 비침습적이거나 덜 침습적인 방법으로 움직임 의도를 정확히 예측하는 BMI 연구가 필요하다. 또한 BMI 시스템을 실생활에서 사용하기 위해서는 사용자가 자신의 필요에 따라 시스템의 모드를 바꿀 수 있어야 한다.

방법: 이를 위해 먼저 비침습적 방법인 뇌자도 신호로부터 3 차원 팔 움직임을 예측할 수 있는 신호처리 알고리즘을 개발했다. 실험은 9 명의 건강한 피험자를 대상으로 중앙에서 밖으로 목표를 향한 팔 움직임을 수행하는 동안 뇌자도를 측정하였다. 데이터 분석결과에 기반하여 뇌자도로부터 움직임 관련 특징들을 추출하였으며, 다중선형회귀를

사용하여 움직임 속도를 예측하는 알고리즘을 개발하였다. 둘째로 BMI 의 정확도 성능 향상을 위해 되먹임 신호를 이용하여 움직임 예측을 보정하는 알고리즘을 개발하였다. 이 알고리즘은 움직임 예측 방향을 토대로 사물 중에서 목표물을 정하고, 목표물에 잘 도달할 수 있도록 예측된 움직임 경로를 목표물 쪽으로 수정해준다. 셋째로 BMI 모드 변경을 위한 뇌 상태 측정에 사용될 수 있는 팔 움직임 동안 뇌의 기능적 연결성의 변화를 살펴보았다. 시간 흐름에 따른 기능적 뇌 연결성을 살펴보기 위해 상호정보량(MI)을 계산하였다. 마지막으로 연구결과에 따른 결론과 이를 토대로 미래 BMI 시스템의 방향을 제안하였다.

결과:

저주파의 MEG 신호로부터 움직임 속도를 상당히 높은 정확도로 예측할 수 있었다 ($p < 0.001$, mean $r > 0.7$). 그리고 되먹임 신호를 이용하여 움직임 예측 정확도를 모든 피험자에서 유의하게 향상시킬 수 있었으며 ($P < 0.001$), 32.1%의 에러를 줄일 수 있었다. 또한 뇌의 상태에 따라 뇌 연결성이 달라지는 것을 확인할 수 있었다. 게다가 움직임 이전에는 대부분의 운동관련 영역에서 중심성이 증가하는 반면, 움직임 중에는 소뇌와 기저핵의 중심성만이 증가하였다.

결론: 비침습적 뇌자도로부터 움직임 경로를 예측할 수 있었으며, 되먹임 정보를 이용하면 예측 정확성을 상당히 향상시킬 수 있었다. 휴지기와 운동계획, 운동수행에 따라 뇌 연결성이 상당히 달라졌기 때문에 이를 토대로 BMI 의 모드를 변경해 줄 수 있을 것이다. 따라서 뇌의 상태와 되먹임 정보를 결합하여 실질적인 BMI 시스템이 가능해질 것이다.

주요어: 뇌-기계 인터페이스, 움직임 경로 예측, 피드백을 이용한 예측 보정, 운동제어기전, 기능적 뇌 연결성

학번: 2011-30131